JACS
JOURNAL OF THE AMERICAN CHEMICAL SOCIETY
Article
pubs.acs.org/JACS

Mechanism and Selectivity of Cooperatively Catalyzed Meyer–Schuster Rearrangement/Tsuji–Trost Allylic Substitution. Evaluation of Synergistic Catalysis by Means of Combined DFT and Kinetics Simulations

Marcin Kalek*,† and Fahmi Himo*,‡

†Centre of New Technologies, University of Warsaw, Banacha 2C, 02-097 Warsaw, Poland
‡Department of Organic Chemistry, Arrhenius Laboratory, Stockholm University, S-106 91 Stockholm, Sweden

Supporting Information

ABSTRACT: The reaction between propargylic alcohols and allylic carbonates, engaging vanadium and palladium catalysts, is an exemplary case of a cooperatively catalyzed process. This combined Meyer–Schuster rearrangement/Tsuji–Trost allylic substitution clearly illustrates the enormous advantages offered by the simultaneous use of two catalysts, but also the inherent challenges regarding selectivity associated with such a reaction design. These challenges originate from the fact that the desired product of the combined process is formed by a bimolecular coupling of the two substrates activated by the respective catalysts. However, these two processes may also occur in a detached way via the reactions of the catalytic intermediates with the starting propargylic alcohol present in the reaction mixture, leading to the formation of two side-products. Herein, we investigate the overall mechanism of this reaction using density functional theory (DFT) methodology. The mechanistic details of the catalytic cycles for all the individual processes are established. In particular, it is shown that the diphosphine ligand, dppm, used in the reaction promotes the formation of dinuclear palladium complexes, wherein only a single metal center is directly involved in the catalysis. Due to the complexity of the combined reaction network, kinetics simulation techniques are employed in order to analyze the overall selectivity. The simulations directly link the results of the DFT calculations with the experimental data and confirm that the computed free energy profiles indeed reproduce the observed selectivities. In addition, a sensitivity analysis is carried out to assess the importance of the individual steps on the product distribution. The observed behavior of the kinetic network is rationalized, and trends in the reaction outcome upon changing the initial conditions, such as the catalysts amounts and ratio, are discussed. The results provide a general framework for understanding the factors governing the selectivity of the cooperatively catalyzed reactions.

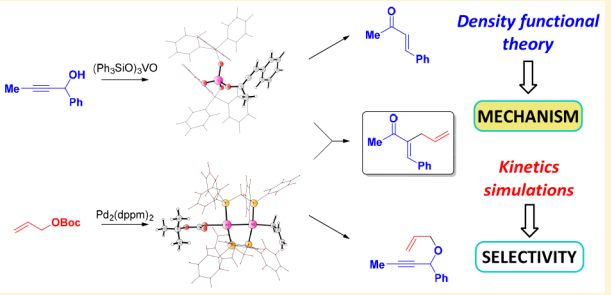

1. INTRODUCTION

Cooperative catalysis has in recent years emerged as a new powerful tool to expand chemical reactivity and to develop new high-performance synthetic methodology.[1] In this approach, which is also referred to as synergistic, dual, or contemporaneous catalysis, two substrates are activated independently with two different catalysts, followed by a coupling between the generated catalytic intermediates. The simultaneous dual activation not only allows for an increase in the reaction rate, permitting efficient coupling of unreactive starting materials, but also enables in many instances completely new, otherwise unattainable transformations.

Selectivity is the major challenge inherently associated with cooperative catalysis. This arises from the fact that the catalytic intermediates that undergo the bimolecular coupling are present in the reaction mixture in low concentrations, while surrounded by a large excess of potentially reactive starting materials. The latter may thus intercept one or both of the intermediates, before the desired coupling occurs, leading to the formation of side-products. Such a reaction network represents a very interesting case from kinetics viewpoint.

One particularly fascinating example of the synergistic catalysis concept was reported by Trost and co-workers (Scheme 1).[2] It clearly demonstrates how the application of this synthetic strategy enables access to unique reactivity patterns and complicated structural motifs. Unlike the majority of the cooperative systems reported so far, which are usually based on a combination of an organocatalyst and a metal catalyst,[1] the reaction shown in Scheme 1 is catalyzed by two transition-metal complexes, and its general mechanism is depicted in Scheme 2.[3] The first catalyst, tris(triphenylsilyl) vanadate, promotes 1,3-transposition of propargylic alcohol **A** to generate nucleophilic vanadium allenoate **C**, whereas the second, palladium(0) complex, undergoes an oxidative addition of allylic carbonate **B** to produce electrophilic π-allyl-palladium

Received: February 24, 2017
Published: July 4, 2017

DOI: 10.1021/jacs.7b01931
J. Am. Chem. Soc. 2017, 139, 10250–10266

Scheme 1. Combined Meyer−Schuster Rearrangement/ Tsuji−Trost Allylic Substitution Catalyzed Cooperatively by Palladium and Vanadium[2]

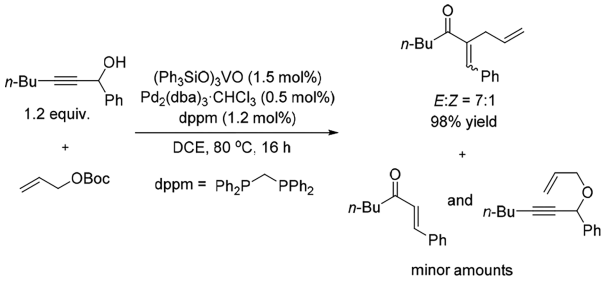

Scheme 2. General Mechanistic Pathways Responsible for the Formation of Different Products in the Cooperatively-Catalyzed Reaction Depicted Scheme 1

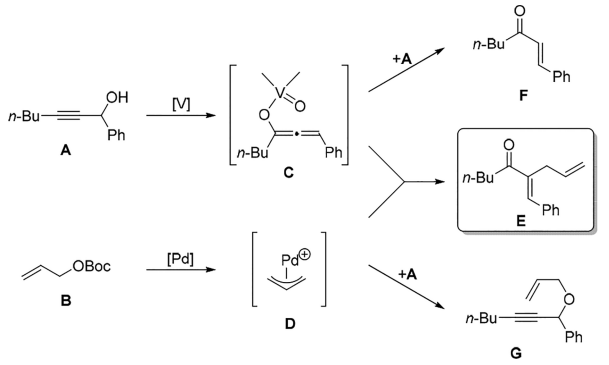

species **D**. In the course of the bimolecular coupling, the reaction between intermediates **C** and **D** yields the desired product, α-allylated α,β-unsaturated ketone **E**. A challenging aspect of this transformation is that both vanadium enolate **C** and the π-allyl-palladium complex **D** can react with another molecule of propargylic alcohol **A**, present in stoichiometric quantities in the reaction mixture, forming the Meyer−Schuster rearrangement[4] and the Tsuji−Trost O-allylation side-products, **F** and **G**, respectively (Scheme 1). Thus, it was argued that for the successful synergistic catalysis to take place, it is necessary that the rate of bicatalytic coupling (**C** + **D** → **E**) is faster than the formation of side-products (**C** + **A** → **F** and **D** + **A** → **G**). In addition, it has been suggested that the rates at which the reactive intermediates **C** and **D** are supplied should be relatively similar, such that overgeneration of one intermediate does not facilitate the side reactions.[2] It was established that in order to obtain the desired product in good selectivity, 1,3-bis-(diphenylphoshino)methane (dppm) had to be applied as the ligand for palladium, and additionally, the ratio of the two catalysts had to be carefully optimized (Scheme 1).[2]

Density functional theory (DFT) calculations can nowadays provide detailed free energy profiles of chemical reactions. The accuracy has been demonstrated to be sufficient to identify and analyze sources of various kinds of selectivities.[5] It can hence be a valuable tool in the study of cooperative catalysis. In the current work, we present a DFT study on the reaction developed by Trost and co-workers. First, the detailed mechanisms are elucidated for each of the three catalytic cycles involved in the overall reaction, i.e., the Meyer−Schuster rearrangement, the O-allylation, and the bicatalytic coupling. A key finding here is that dppm ligand promotes the formation of dinuclear palladium complexes, with one metal playing the role of a reacting center, while the other being a spectator. Due to the complexity of the mechanism, the selectivity cannot be established by simple analysis of the obtained free energy profiles or by methods based on the steady-state approximation.[6] Therefore, we apply kinetics simulations in order to link the results of the calculations with the experimental data. This approach confirms that the computed energies indeed reproduce the observed trends in selectivity and enable a detailed analysis in order to assess the importance of the individual steps on the final outcome of the process.

2. COMPUTATIONAL METHODS

The DFT calculations were performed with the B3LYP functional[7] as implemented in Gaussian 09 package.[8] Geometries were optimized using 6-31G(d,p) basis set for C, H, O, P, and Si, and the LANL2DZ pseudopotential[9] for Pd and V. The calculations were carried out using the full structures of reagents and catalysts as shown in Scheme 1, with the exception of propargylic alcohol, in which the *n*-butyl substituent was replaced by a methyl group. For each stationary point a thorough conformational analysis was performed in order to locate the conformer with the lowest energy. This was done by identifying key rotatable bonds and manually building possible starting geometries for optimizations. In the case of the largest structures (>200 atoms), due to the immense number of possible conformers, we followed a slightly different procedure in which the most drastic conformational changes were evaluated first, followed by a more careful fine-tuning of selected lowest energy conformational branches (corresponding to testing a total of 20−50 structures for each stationary point). This procedure is expected to cover the bulk of the conformational space and provide reliable energy values, although with a slightly higher error bar.

The identified lowest energy stationary points were then characterized by frequency calculations to confirm their character as minima (no imaginary frequencies) or transition states (one single imaginary frequency). The final Gibbs free energies reported in this article were obtained from single-point calculations using the larger basis set 6-311+G(2d,2p) for C, H, O, P, and Si, and LANL2TZ(f) for Pd and V, corrected for zero-point and thermal effects at 333.15 K from the frequency calculations (60 °C was the temperature of optimization experiments),[2] dispersion effect using the B3LYP-D3 method of Grimme,[10] and solvation free energy. The latter was calculated as a single-point correction on the optimized structures using the conductor-like polarizable continuum model (CPCM)[11] method with the parameters for dichloroethane (DCE). Although the various steps of this adopted computational scheme are quite standard in the field, it is important to bear in mind that they could be associated with some errors, as has been discussed recently by Plata and Singleton.[12]

The kinetics simulations were carried out using the LSODA algorithm[13] (from ODEPACK library)[14] for integration of ordinary differential equations as implemented in COPASI software (version 4.16, build 104).[15]

3. RESULTS AND DISCUSSION

The overall transformation depicted in Scheme 1 consists of three different processes: (1) vanadium-catalyzed Meyer−Schuster rearrangement, producing α,β-unsaturated ketone, (2) palladium-catalyzed Tsuji−Trost O-allylation of propargylic alcohol, leading to allyl propargyl ether, and (3) the

Scheme 3. Vanadium-Catalyzed Meyer−Schuster Rearrangement of Propargylic Alcohol 1, the First Undesired Side-Process in the Cooperatively Catalyzed Reaction

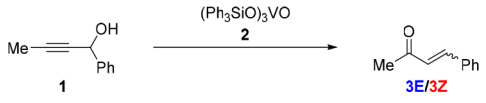

DOI: 10.1021/jacs.7b01931
J. Am. Chem. Soc. 2017, 139, 10250−10266

Scheme 4. Mechanism of the Vanadium-Catalyzed Meyer–Schuster Rearrangement (Cycle I) Established by Previous Calculations[16]

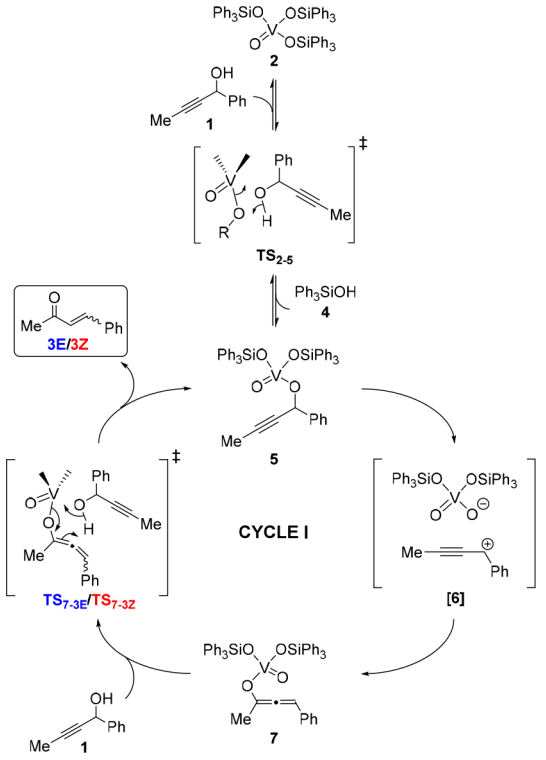

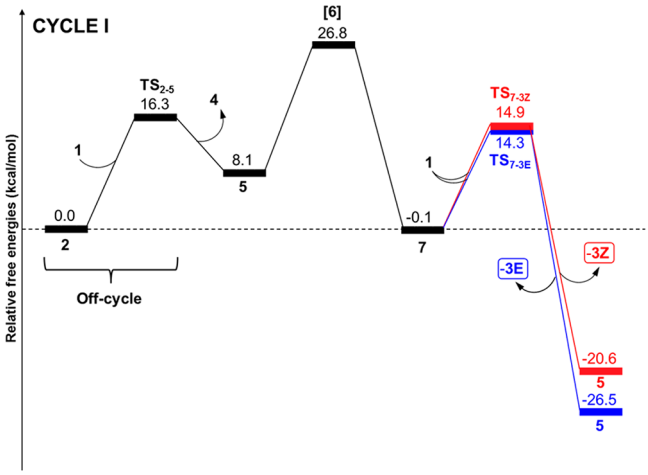

Figure 1. Free energy profile for the vanadium-catalyzed Meyer–Schuster rearrangement.

cooperatively catalyzed pathway, involving the coupling of two catalytic intermediates and yielding the desired reaction product.

In this section, we first present the investigations on the mechanisms of all these processes one by one. Importantly, before proceeding to the catalytic cycles involving palladium, we perform an exploratory study to establish the preferred coordination of palladium complexes containing dppm ligand. Next, the full combined mechanism of the reaction is studied using the kinetics simulation technique to provide the product distribution based on the calculated energies. Finally, we perform a sensitivity analysis to uncover the origins of the selectivity and factors that control it.

Scheme 5. Various Monomeric and Dimeric dppm-Palladium(0) Complexes That Can Form in the Presence of the Reaction Substrates[a]

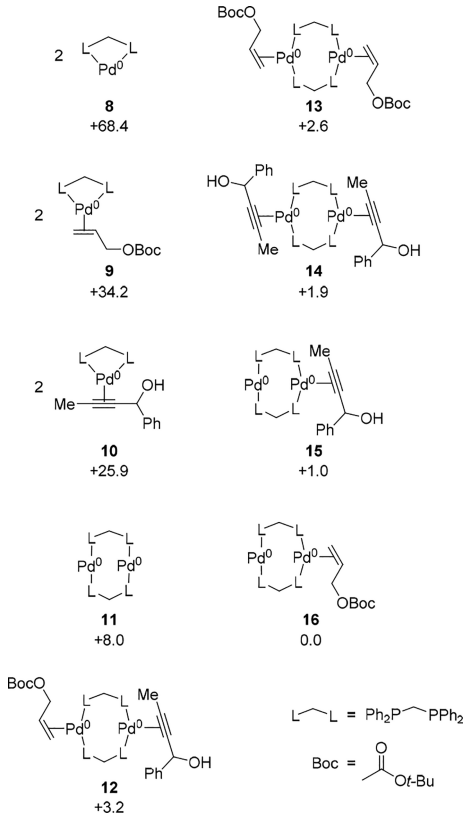

[a]Calculated energies relative to the lowest energy complex **16** are indicated in kcal/mol.

3.1. Vanadium-Catalyzed Meyer–Schuster Rearrangement. We have previously reported a detailed mechanistic investigation of the vanadium-catalyzed Meyer–Schuster rearrangement (Scheme 3).[16] The most important features of the mechanism are summarized in this section. For consistency with the other parts of the current study, the energies were slightly refined by using the D3 dispersion correction instead of the D2 that was used in the original study.[16] This gives slightly different energy values, but does not affect the general conclusions regarding the mechanism.

It was established that the vanadium-catalyzed Meyer–Schuster rearrangement is a three-step process (Scheme 4, Cycle I) involving: (1) incorporation of the propargylic alcohol **1** into the vanadium complex by exchange of one of the triphenylsiloxy ligands in catalyst **2**; (2) dissociative 1,3-oxygen shift, yielding vanadium allenoate **7**; and (3) simultaneous transesterification/tautomerization ($\mathbf{TS}_{7-3E}$/$\mathbf{TS}_{7-3Z}$), producing ketones **3E** and **3Z** and regenerating vanadium alkoxide intermediate **5**. The corresponding calculated free energy diagram for this reaction is shown in Figure 1.

The calculations showed that only one propargylic alkoxide ligand is incorporated into the vanadium complex (introduction of more alkoxide moieties leads to higher energies), and the process is endergonic by 8.1 kcal/mol. The ligand exchange takes place via σ-bond metathesis ($\mathbf{TS}_{2-5}$). As indicated above, the key 1,3-oxygen shift was found to occur preferentially by a dissociative mechanism with the intermediacy of ion-pair **6**. Such a course of reaction causes loss of stereochemical

DOI: 10.1021/jacs.7b01931
J. Am. Chem. Soc. 2017, 139, 10250–10266

Scheme 6. Overview of Complexes with $(dppm)_2Pd_2$ Core That May Form in the Presence of Allylic Carbonate 17[a]

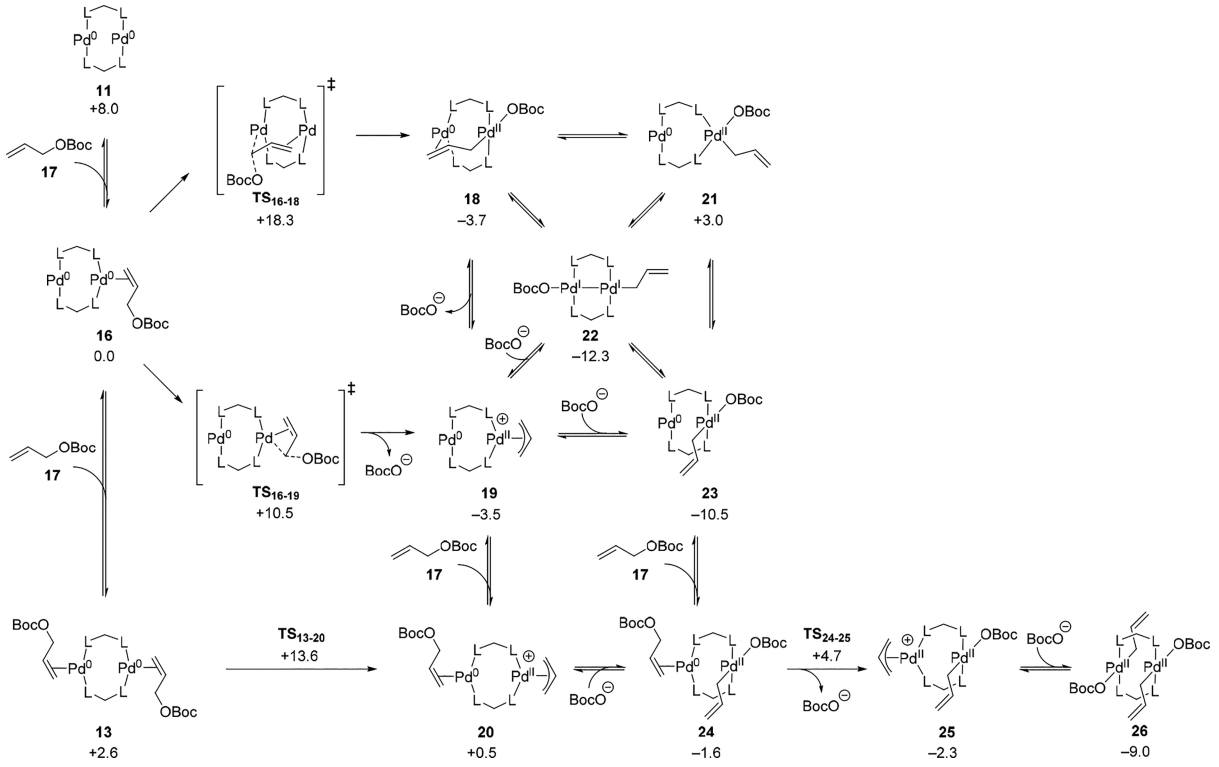

[a]Calculated energies of the intermediates and transition states are given in kcal/mol relative to complex **16**.

information from the chiral propargylic alcohol **1**, since the ions may recombine in a nonstereoselective manner. Hence, allenoate **7** is always formed as a racemate, even if enantiopure alcohol **1** is used as a substrate. Finally, it was established that **7** is directly converted into ketones **3E** and **3Z**, without intermediate formation of a free enol. The transition states for this transformation (TS_{7-3E} and TS_{7-3Z}) involve a concerted proton transfer from alcohol **1** (in a six-membered cyclic structure) directly to the α-carbon atom of the leaving group. Simultaneously, a ligand exchange at the vanadium center takes place. Since the transition states leading to the isomeric ketones **3E** and **3Z** have very similar energies (0.6 kcal/mol difference between TS_{7-3E} and TS_{7-3Z}), a mixture of these products should be formed, which is indeed the result observed experimentally.[2a] The overall thermodynamics of the reaction, corresponding in Figure 1 to a full turnover of the catalytic cycle from intermediate **5** back to intermediate **5**, is calculated to be −28.7 and −34.6 kcal/mol for the formation of products **3E** and **3Z**, respectively.

The mechanism of Scheme 4 was thus found to be consistent with all available experimental facts known about the vanadium-catalyzed Meyer−Schuster rearrangement.[4,17]

3.2. Coordination of Palladium in Complexes with dppm Ligand. The second process involved in mechanism of the transformation shown in Scheme 1 is the palladium-catalyzed Tsuji−Trost reaction, which is responsible for both the formation of the desired product and the side O-allylation of propargylic alcohol (**E** and **G** in Scheme 2, respectively). Many variations of the palladium-catalyzed allylic substitution have been studied both experimentally[18] and theoretically.[19] However, there are a number of important aspects that distinguish the current reaction from these studies, rendering it necessary to conduct a detailed mechanistic investigation. The first point that deserves special attention and that will be addressed in this section is that the reaction makes use of dppm as a supporting ligand for palladium. There are no other examples of the application of this ligand in the Tsuji−Trost reactions.[20] The distinctive feature of dppm is that it is known to promote the formation of dinuclear palldium complexes,[21] although mononuclear palladium complexes with a chelating dppm ligand have also been characterized crystallographically.[22] Additionally, a possible interconversion between the two types of complexes has been suggested to take place under certain conditions.[21e]

Therefore, we started the investigations by examining which kind of species, mono- or dipalladium, is preferentially formed in the reaction mixture and participates in the current transformation. Scheme 5 depicts a comparison of the calculated energies of putative palladium(0) complexes that can possibly exist in the reaction mixture containing dppm ligand and the unsaturated substrates (allylic carbonate **17** and propargylic alcohol **1**), corresponding to the situation at the outset of the reaction.[23] It is clear from the calculated energies that the formation of the dinuclear complexes (**11**−**16**) is strongly preferred compared to the mononuclear ones (**8**−**10**). A plausible explanation for this is that the four-membered metalacycle in the monomeric complexes is highly strained, compared to a more relaxed eight-membered ring in the dimeric counterparts. Because of the large energetic preference for the formation of dipalladium dppm complexes, the involvement of monomeric species in the mechanism can be excluded, and it will not be considered any further here. Regarding the relative stability of the different dinuclear species, the coordination of one unsaturated ligand to the generic Pd(0)−Pd(0) complex **11** is favorable (**15** and **16**), whereas the coordination of the second one is slightly energetically

DOI: 10.1021/jacs.7b01931
J. Am. Chem. Soc. 2017, 139, 10250−10266

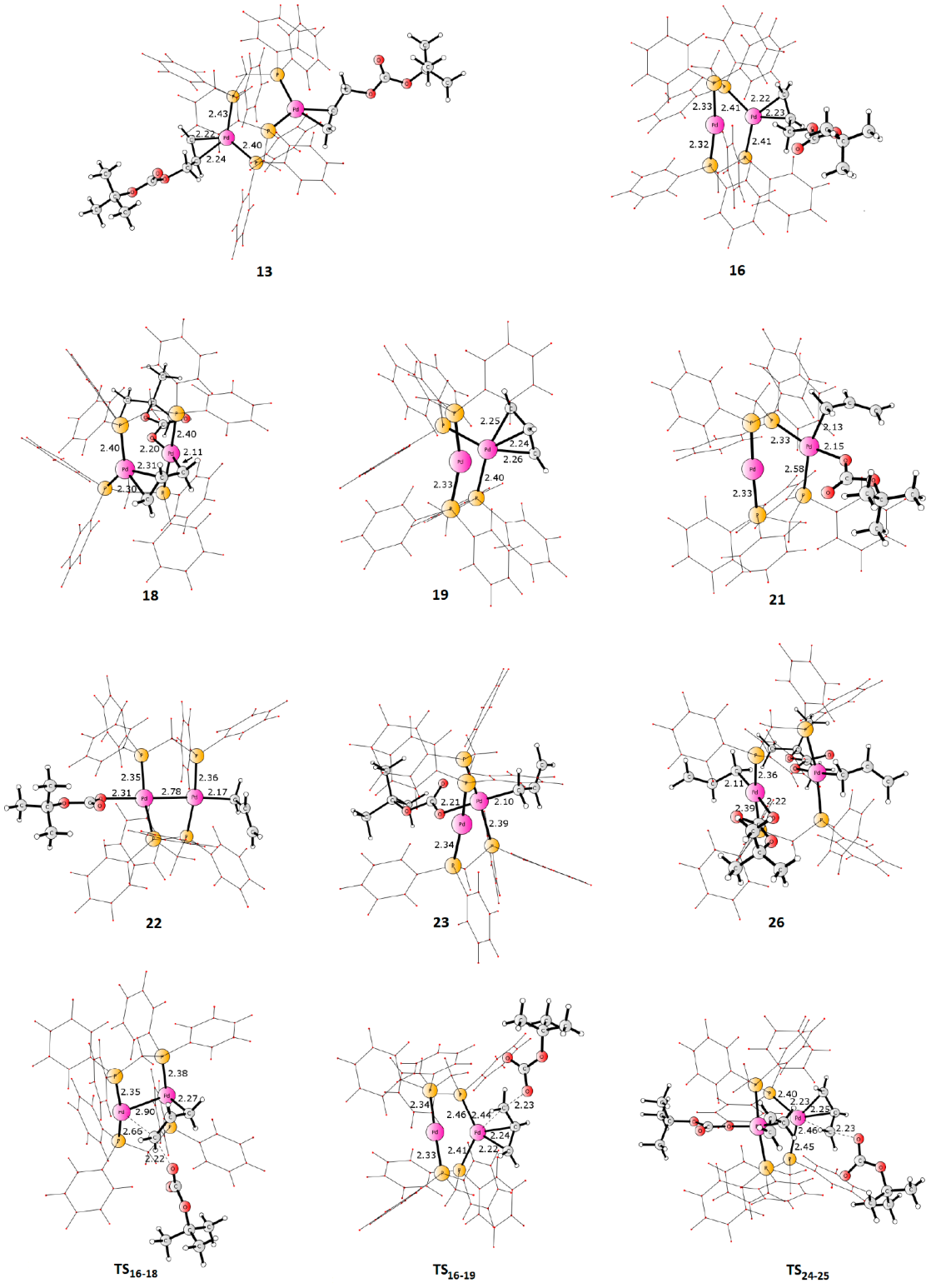

Figure 2. Optimized structures of selected intermediates and transitions states from Scheme 6. The backbones and phenyl groups of dppm ligands are shown in a simplified fashion for clarity. Distances are given in Å.

uphill (**12**−**14**), irrespective of the nature of the ligand involved (**17** or **1**). Since the formation of palladium complexes with propargylic alcohol **1** is mechanistically unproductive (they are not reactive intermediates), the only role that such species could potentially play is to be the resting state of the palladium catalyst. However, all evaluated complexes of this type (**12**, **14**, and **15**) are higher in energy than complex **16**, containing the allylic carbonate substrate, and their engagement in the mechanism can therefore be disregarded.

Due to the presence of two palladium atoms in the dinuclear complexes, one can envision two different ways by which the activation of allylic carbonate **17** may operate. Namely, either both metal centers are directly involved in the process by a simultaneous binding of the reactants, or alternatively, the

DOI: 10.1021/jacs.7b01931
J. Am. Chem. Soc. 2017, 139, 10250−10266

Scheme 7. Palladium-Catalyzed O-Allylation of Propargylic Alcohol 1, the Second Undesired Side-Process in the Cooperatively Catalyzed Reaction

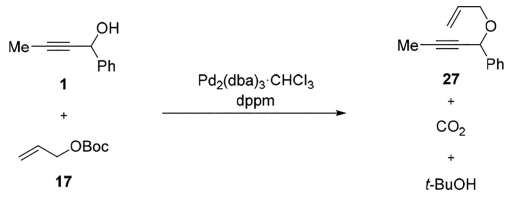

transformation occurs only at one of the palladium centers, while the other remains a spectator. In the latter case, the most stable form of the spectator has to be determined. Importantly, this form may be different for the different processes occurring at the "active" metal center. Likewise, it is also possible that the pathway engaging two palladiums is energetically preferred in certain steps, while for others, the one with a single reaction center is favored.

To gain deeper insight into the mechanism, we optimized the structures and calculated the energies of a number of conceivable intermediates and transition states that may be attained in the presence of the allylic carbonate substrate. The obtained results are summarized in Scheme 6, where the calculated energies are given relative to complex **16**, which turned out to be the most stable Pd(0)−Pd(0) species. Optimized structures of selected intermediates and transition states are depicted in Figure 2.

As shown in Schemes 5 and 6, complexes **16** and **13** are close in energy and both of them may therefore undergo oxidative addition. In the case of complex **16**, we located two different transition states for the oxidative addition. The first one ($\mathbf{TS_{16-18}}$) engages both palladium centers simultaneously and requires overcoming a barrier of 18.3 kcal/mol. It leads to complex **18**, wherein one of the metals has a square-planar Pd(II) character with the carbonate anion and σ-allyl ligands in *trans* arrangement, while the other is a Pd(0) coordinated to the pending olefin.[24] The formation of **18** is slightly exergonic (−3.7 kcal/mol relative to **16**). The oxidative addition proceeding via the other transition state, $\mathbf{TS_{16-19}}$, occurs exclusively at one metal center and has a considerably lower barrier of 10.5 kcal/mol. This transformation produces a cationic π-allyl complex **19**[25] that is very close in energy to **18** (−3.5 kcal/mol relative to **16**).

The oxidative addition may also take place from complex **13**, containing two coordinated reactants, via a transition state $\mathbf{TS_{13-20}}$ similar to $\mathbf{TS_{16-19}}$, but with a different spectator center. The calculated energy of $\mathbf{TS_{13-20}}$ is 13.6 kcal/mol relative to **16**, which is 3.1 kcal/mol higher than $\mathbf{TS_{16-19}}$.

Complexes **18**−**20** are thus close in energy, and interconversion between them is kinetically feasible since it only involves the coordination/decoordination of the $BocO^-$ anion and olefin ligands to/from the metal centers (including the associated changes between σ- and π-coordination modes of the allyl moiety). More importantly, such ligand exchange processes provide access to a number of other complexes that may possibly form in the reaction mixture and remain in a fast equilibrium. Therefore, we have evaluated the energies of additional conceivable species **21**−**24** shown in Scheme 6. One important general conclusion from these results about the structure−stability relationship of the complexes with a $(dppm)_2Pd_2$ core is that the eight-membered dipalladacycle prefers strongly to remain in an approximately planar geometry, with P−Pd−P angles close to 180°. Any significant distortion from the linearity results in a destabilization. This feature manifests itself in a number of ways. First, the square-planar Pd(II) center preferentially adopts a configuration with the L groups of dppm ligands (PPh_2) in a *trans* arrangement. Thus, complex **23** is considerably more stable than its *cis* isomer **21** as well as complex **19**, in which the L groups are also forced to be *cis* to each other due to the presence of a π-allyl ligand. Second, the coordination of an unsaturated ligand to a palladium(0) center, necessarily resulting in the bending of P−Pd−P angle, is also disfavored to the point of overweighing the energy gained by the coordination. For instance, complex **23** is 6.8 kcal/mol more stable than complex **18** with the internal coordination present and 8.9 kcal/mol more than complex **24**, containing an additional allyl carbonate ligand. The difference in energy between $\mathbf{TS_{16-19}}$ and $\mathbf{TS_{16-18}}$ (7.8 kcal/mol), as well as between $\mathbf{TS_{16-19}}$ and $\mathbf{TS_{13-20}}$ (3.1 kcal/mol), is likely to be of similar origin. Finally, following the same reasoning, the Pd(I)−Pd(I) complex **22**, encompassing both the advantageous unstrained *trans*-L,L geometry and an additional interaction between the metal centers (Pd−Pd distance: 2.78 Å), can be identified to be the most stable complex. This is in line with many experimental observations of similar complexes, containing $(dppm)_2Pd_2$ core.[21] In fact, **22** is also the most stable structure among all palladium species present in the reaction mixture, and it constitutes thus the catalyst resting state, as will be discussed below.

To complete the picture, we have also evaluated the formation of Pd(II)−Pd(II) complexes via a second oxidative addition of allyl carbonate **17**. Only a transition state $\mathbf{TS_{24-25}}$ originating from complex **24** was considered, containing the spectator Pd(II) center in the most stable configuration, as determined above. The energy of the TS is calculated to be 4.7 kcal/mol relative to **16**, which corresponds to an overall barrier of 17.0 kcal/mol from the lowest energy species **22**. The direct product of $\mathbf{TS_{24-25}}$ is a π-allyl complex **25**. It can, however, interconvert into a more stable (by 6.7 kcal/mol) complex **26**, containing two σ-allyl ligands. Thus, under the reaction conditions, the generation of Pd(II)−Pd(II) complexes is a viable option, and their involvement in the mechanism needs therefore to be examined.

To summarize this section, a broad exploration has been carried out of palladium complexes with dppm ligand that can form in the presence of allylic carbonate **17** and propargylic alcohol **1**. It is found that dinuclear species are strongly preferred compared to mononuclear ones. We were able to establish a general principle governing the relative stability of complexes with $(dppm)_2Pd_2$ core and identify the Pd(I)−Pd(I) compound **22** as the most stable structure. The calculations show that there are two kinetically feasible pathways by which the allylic carbonate can be activated via the oxidative addition. The first one operates between Pd(0)−Pd(0) and Pd(0)−Pd(II) species, through $\mathbf{TS_{16-19}}$, and the second involves the transformation between Pd(0)−Pd(II) and Pd(II)−Pd(II) intermediates, via $\mathbf{TS_{24-25}}$. Both of these alternatives will therefore be evaluated in the context of the investigated cooperatively catalyzed reaction.

3.3. Palladium-Catalyzed O-Allylation of Propargylic Alcohol 1. The specific case of palladium-catalyzed Tsuji−Trost reaction involving alcohol nucleophiles, such as the one responsible for the formation of allyl propargyl ether side-product (Scheme 7), has not been directly investigated by computations previously. Therefore, we first examined a

DOI: 10.1021/jacs.7b01931
J. Am. Chem. Soc. 2017, 139, 10250−10266

Scheme 8. Conceivable Mechanisms for the Formation of Allyl-Propargyl Ether 27: Pd(0)−Pd(0)/Pd(0)−Pd(II) Cycle (Cycle II) and Pd(0)−Pd(II)/Pd(II)−Pd(II) Cycle (Cycle III)[a]

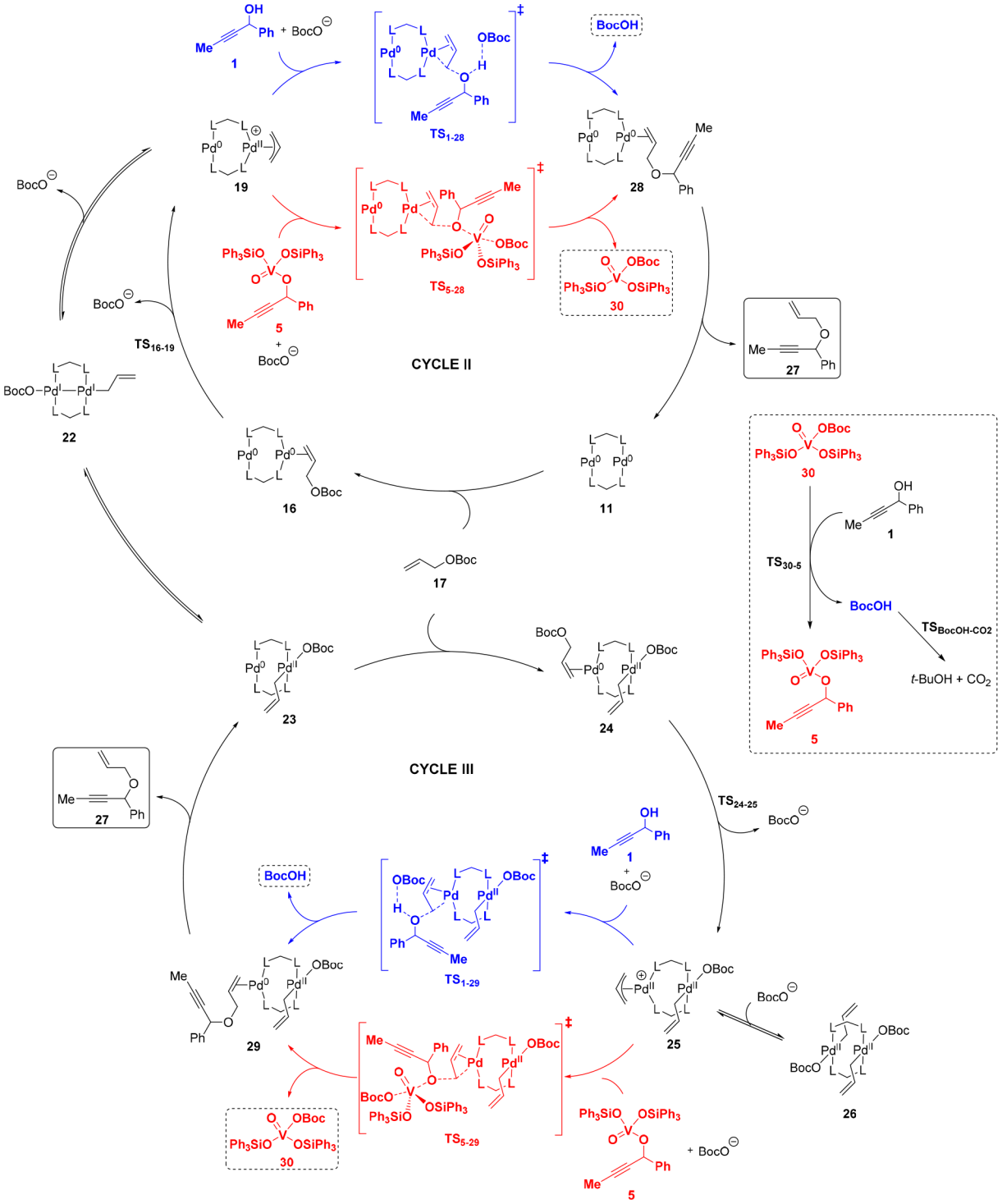

[a]The pathways involving free alcohol **1** nucleophile are shown in blue and the ones involving vanadium alkoxide **5** nucleophile in red. The off-cycle regeneration of the reactive vanadium species and decarboxylation of BocOH are depicted in the inset.

number of general mechanistic possibilities for the C−O bond formation using monomeric palladium complexes as models. These investigations are reported in the Supporting Information. The calculations could establish that there are two general pathways that may possibly be responsible for the C−O bond formation. The first one involves a nucleophilic attack of free propargylic alcohol **1** on the π-allyl palladium complex, occurring with a simultaneous deprotonation by a carbonate anion. In the second mechanism, vanadium alkoxide **5** acts as the nucleophile instead, attacking the π-allyl. Importantly, in the latter case, the alkoxide ligand is simultaneously displaced by the carbonate anion at the vanadium center in an S_N2 fashion via a trigonal-bipyramidal transition state. The other examined

DOI: 10.1021/jacs.7b01931
J. Am. Chem. Soc. 2017, 139, 10250−10266

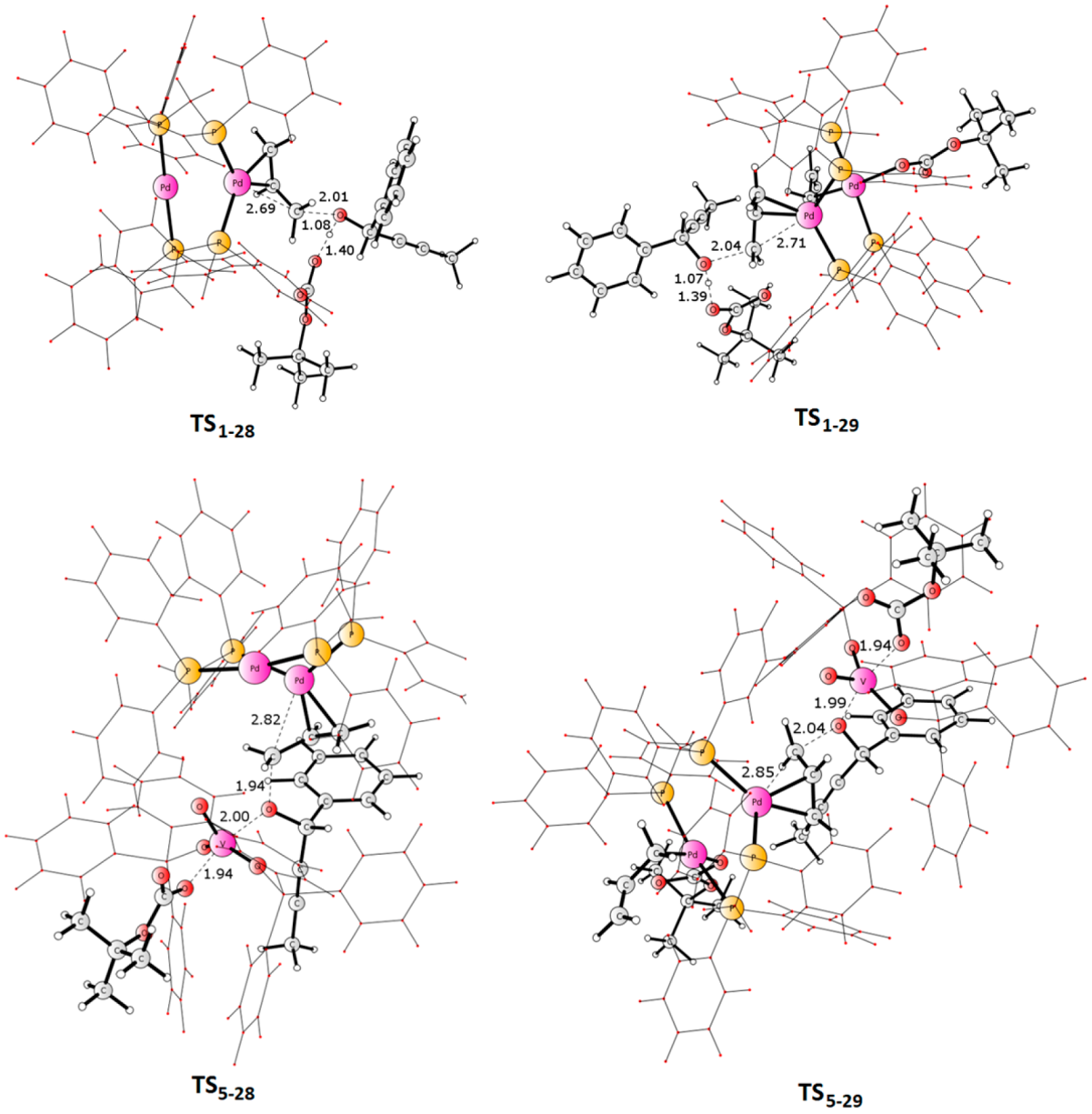

Figure 3. Optimized structures of transitions states for the formation of allyl-propargyl ether **27**. The backbones and phenyl groups of dppm ligands as well as Ph_3Si groups of vanadium catalyst are shown in a simplified fashion for clarity. Distances are given in Å.

pathways were not found to be feasible (see the Supporting Information for details).

Applying this knowledge in the context of dinuclear palladium species and taking into account the results described in the previous section, regarding the preferred coordination modes of complexes with $(dppm)_2Pd_2$ core, implies that there are as many as four conceivable pathways for the formation of allyl-propargyl ether **27** (Scheme 8).

The first two of them engage Pd(0)−Pd(0) and Pd(0)−Pd(II) species (Scheme 8, Cycle II), with the key C−O forming transition states originating at π-allyl complex **19**. Depending on the identity of the nucleophile, these are $\mathbf{TS}_{1-28}$, involving free alcohol **1** (in blue at the top of Scheme 8), and $\mathbf{TS}_{5-28}$, involving vanadium alkoxide **5** (in red at the top Scheme 8; see Figure 3 for optimized structures). The spectator palladium(0) center remains two-coordinate throughout the cycle, since the introduction of any additional ligands destabilizes the system, as shown above. In the other two possible mechanisms, the oxidation state of the complexes alternates between Pd(0)−Pd(II) and Pd(II)−Pd(II) (Scheme 8, Cycle III). The C−O bond is formed by the nucleophilic attack of either free alcohol **1** ($\mathbf{TS}_{1-29}$, in blue at the bottom of Scheme 8) or vanadium alkoxide **5** ($\mathbf{TS}_{5-29}$, in red at the bottom of Scheme 8) on the π-allyl ligand in intermediate **25** (Figure 3). In this case, the spectator part is a Pd(II) center with σ-allyl and BocO ligands in the most stable *trans* arrangement. After the C−O bond is formed, the cycles are closed by exchanging the coordinated product **27** to another molecule of reactant **17**. Importantly, all the mechanisms share the same Pd(I)−Pd(I) resting state **22**, located outside the cycles. Its transformation into the reactive π-allyl complex in the Pd(0)−Pd(0)/Pd(0)−Pd(II) cycle, **19**, requires the dissociation of $BocO^-$ anion. On the other hand, in order to join the Pd(0)−Pd(II)/Pd(II)−Pd(II) cycle, **22** needs to interconvert into complex **23**. A possible reversible formation of bis(σ-allyl) species **26**, another low-energy off-

DOI: 10.1021/jacs.7b01931
J. Am. Chem. Soc. 2017, 139, 10250−10266

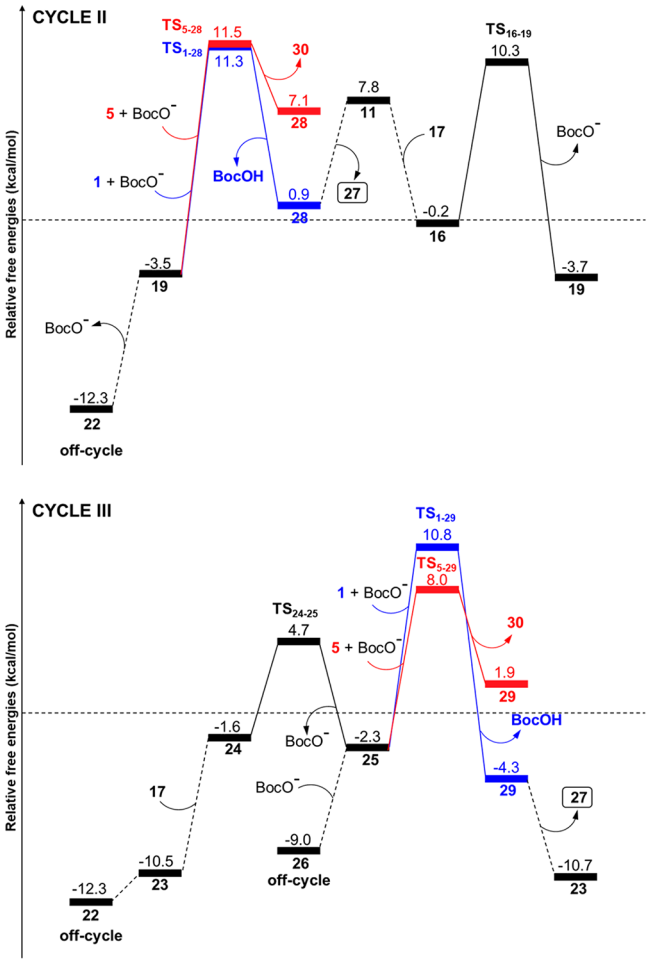

Figure 4. Free energy profiles for the palladium part of O-allylation of propargylic alcohol **1** via Pd(0)−Pd(0)/Pd(0)−Pd(II) (Cycle II) and Pd(0)−Pd(II)/Pd(II)−Pd(II) (Cycle III) intermediates. Note that profiles for the full catalytic turnover are only shown for the mechanisms with BocOH side-product (see the text for discussion).

Scheme 9. Cooperatively Catalyzed Combined Meyer−Schuster Rearrangement and Tsuji−Trost Reaction

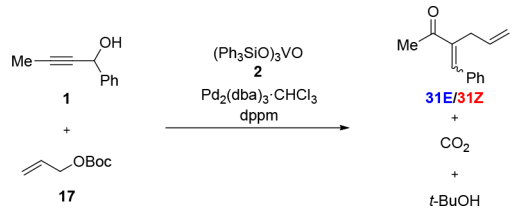

cycle intermediate, from complex **25** has also been included into the mechanism to complete the picture.

The mechanisms involving vanadium alkoxide **5** as the nucleophile ($\mathbf{TS_{5-28}}$ and $\mathbf{TS_{5-29}}$) are catalyzed cooperatively by both metals, and thus, apart from appropriate palladium complexes, they produce vanadium species (t-BuOCO$_2$)-(Ph$_3$SiO)$_2$VO (**30**). In order to regenerate the active form of vanadium catalyst **5** and close the vanadium catalytic cycle, an exchange of the carbonate ligand in intermediate **30** with a propargylic alcohol moiety must take place. We found that such a transformation occurs via transition state $\mathbf{TS_{30-5}}$ that is similar to $\mathbf{TS_{2-5}}$, i.e., the ligand substitution takes place by a σ-bond metathesis (inset in Scheme 8). This process as well as the C−O bond formations with free alcohol **1** nucleophile ($\mathbf{TS_{1-28}}$ and $\mathbf{TS_{1-29}}$) yield carbonic acid monoester, BocOH, which undergoes a decarboxylation, also outside of the catalytic cycles ($\mathbf{TS_{BocOH-CO_2}}$).

The calculated free energy profiles corresponding to these alternative mechanisms are compared in Figure 4. For all cases, the largest energy spans are located between the Pd(I)−Pd(I) complex **22** and the transition states for the C−O bond formation (23.6, 23.8, 23.1, and 20.3 kcal/mol for $\mathbf{TS_{1-28}}$, $\mathbf{TS_{5-28}}$, $\mathbf{TS_{1-29}}$, and $\mathbf{TS_{5-29}}$, respectively). Hence, the lowest energy Pd(II)−Pd(II) intermediate **26** does not constitute the resting state of Cycle III, but it will exist in an equilibrium with the global resting state **22**. Here, it must be stressed that the direct comparison of the barriers in the free energy diagrams in Figure 4 is not possible due to the large differences in concentrations of the various entities present in the reaction mixture. In particular, alcohol **1** is present in the reaction mixture in much higher concentration than catalytic intermediate **5**. Thus, despite the fact that both of these species display comparable intrinsic reactivities toward the nucleophilic attack on π-allyl complexes **19** and **25** (within 5 kcal/mol difference), the relative contributions of these alternative pathways to the overall formation of product **27** will be quite different. Hence, the efficiencies of the different mechanisms and catalytic cycles can only be fully evaluated by kinetics simulations, as will be discussed below.

Another obstacle in the interpretation of Figure 4 is that the regeneration of vanadium alkoxide **5** ($\mathbf{TS_{30-5}}$) takes place off-cycle, in an independent fashion (the barrier for this step is calculated to be 13.6 kcal/mol). Thus, the 6.2 kcal/mol energy difference between intermediate **28** generated by $\mathbf{TS_{1-28}}$ (in blue) and the same intermediate generated by $\mathbf{TS_{5-28}}$ (in red) in Cycle II originates from the thermodynamics of the transformation of **30** into BocOH via $\mathbf{TS_{30-5}}$ (the same applies to intermediates **29** in Cycle III). Therefore, for simplicity, in Figure 4 we have arbitrarily only indicated the complete free energy profiles for full catalytic turnovers for the mechanisms with BocOH side-product. The results demonstrate that the catalytic turnover for the formation of ether **27** is practically thermoneutral (−0.2 kcal/mol, from **19** to **19** or from **23** to **23** in Cycles II and III, respectively). Very importantly, however, the decarboxylation of carbonic acid monoester, BocOH, also taking place independently outside the catalytic cycles ($\mathbf{TS_{BocOH-CO2}}$), is very facile (with a barrier of only 14.0 kcal/mol[26] relative to BocOH) and exergonic by 17.3 kcal/mol. Hence, this process renders the C−O bond-formation irreversible, and it provides the driving force for the overall reaction shown in Scheme 7.

3.4. Cooperatively Catalyzed Combined Reaction. The final and most important part of the mechanism is the coupling of the catalytic palladium and vanadium intermediates, effecting the C−C bond formation and affording the desired reaction product (Scheme 9).

As in the case of the Tsuji−Trost reaction discussed above, we have first evaluated possible general pathways via which this process may occur using monomeric complexes serving as models (see the Supporting Information for details). These calculations could establish that a direct nucleophilic attack of vanadium enolate on palladium π-allyl complex is by far the energetically most favorable alternative. Similarly as in the O-allylation described in the previous section, in order for the attack to have a plausible barrier, it must take place with a

DOI: 10.1021/jacs.7b01931
J. Am. Chem. Soc. 2017, 139, 10250−10266

Scheme 10. Mechanisms of Palladium-Catalyzed Allylation of Vanadium Enolate 6 Occurring via Pd(0)−Pd(0)/Pd(0)−Pd(II) Cycle (Cycle IV) and Pd(0)−Pd(II)/Pd(II)−Pd(II) Cycle (Cycle V)

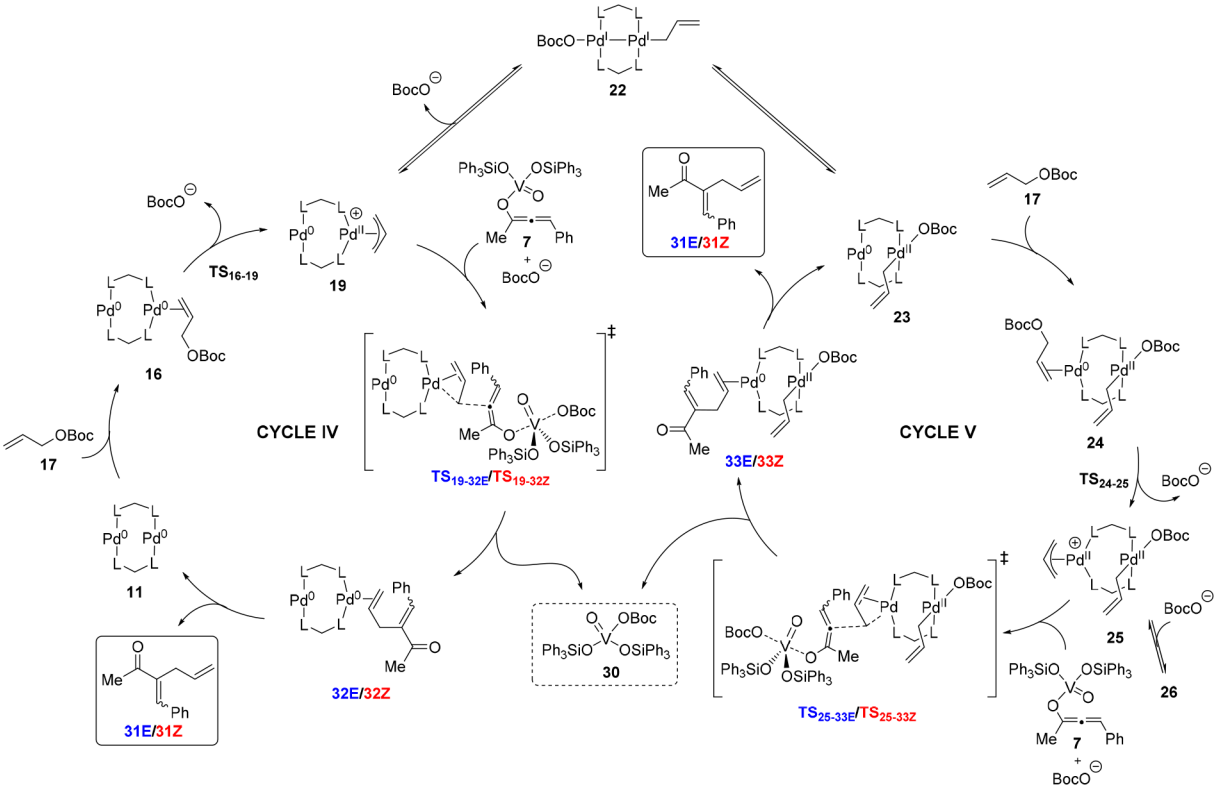

simultaneous displacement of the leaving group by the carbonate anion at the vanadium center in an S_N2 fashion via a trigonal-bipyramidal transition state. The attack of vanadium enolate on the π-allylpalladium taking place without the ligand exchange at vanadium leads to the formation of a charged intermediate, and the corresponding transition state was found to have high energy. We have also examined the possibility that the C−C bond is formed via a reductive elimination of the σ-allyl and C-enolate ligands from palladium center, but this pathway was also found to proceed via a high-energy transition state (see SI).

On the basis of these results, and analogously to the C−O bond formation during the O-allylation of propargylic alcohol **1** described in the previous section, the key C−C bond formation in the bicatalytic pathway may thus involve either intermediate **19**, containing a two-coordinate Pd(0) spectator, or intermediate **25** with a four-coordinate Pd(II) spectator (Scheme 10, Cycles IV and V, respectively). The calculated free energy diagrams for both these mechanistic alternatives are shown in Figure 5, and the optimized structures of the key transition states are depicted in Figure 6.

Although the catalytic cycles shown in Schemes 8 and 10 show a high degree of similarity, the two processes are quite different from each other from energetic point of view. The most striking differences are the very low barriers for the key C−C bond formation, compared to those for the C−O bond formation. Namely, transition states $\mathbf{TS_{19-32E}}$/$\mathbf{TS_{19-32Z}}$ and $\mathbf{TS_{25-33E}}$/$\mathbf{TS_{25-33Z}}$ are only 2.6−3.7 kcal/mol higher in energy than the preceding intermediates **19** and **25**, compared to 10.3−15.0 kcal/mol calculated above for $\mathbf{TS_{1-28}}$, $\mathbf{TS_{5-28}}$, $\mathbf{TS_{1-29}}$, and $\mathbf{TS_{5-29}}$. Therefore, there seems to be a very good match between the electrophilic reactivity of the palladium π-allyl complex and the nucleophilic reactivity of the vanadium enolate. It is also important to remark that the C−C bond formation involving a mononuclear palladium π-allyl complex (with dppe ligand) displays noticeably higher barriers of 10.4−12.1 kcal/mol.[27] Hence, the dinuclear complexes with $(dppm)_2Pd_2$ core are inherently well suited for promoting this key step of the reaction. The high mutual affinity between the palladium and vanadium intermediates, enabling an extremely efficient coupling, is essential for the success of the cooperatively catalyzed process, as it compensates for the very low concentrations of the catalytic intermediates **19**, **25**, and **7** present in the reaction mixture. Again, the large differences in concentrations of the various species present in the reaction mixture make the direct comparison of the free energy diagrams in Figure 5 difficult. In particular, despite a noticeably lower largest energy span in Cycle IV (11.9/12.5 kcal/mol between **22** and $\mathbf{TS_{19-32E}}$/$\mathbf{TS_{19-32Z}}$), compared to that in Cycle V (17.0 kcal/mol between **22** and $\mathbf{TS_{24-25}}$), the latter mechanism may still contribute considerable amounts of products **31E** and **31Z**, as will be demonstrated by the kinetics simulations in the following section.

As to the difference in energy between the transition states leading to (*E*)- and (*Z*)-products, the calculated values, 0.6 for $\mathbf{TS_{19-32E}}$ vs $\mathbf{TS_{19-32Z}}$ and 1.1 kcal/mol for $\mathbf{TS_{25-33E}}$ vs $\mathbf{TS_{25-33Z}}$, corresponding to 2.4:1 and 5.0:1 (*E*):(*Z*)-ratios at 60 °C, respectively, adhere well to the experimentally observed 3:1−6:1 (*E*):(*Z*)-selectivities[2] (see the next section for the cumulative (*E*):(*Z*)-selectivities obtained from kinetics simulations). It might seem surprising that the formation of (*E*)-product is preferred, considering that it requires the approach of the π-allyl complex from the phenyl-substituted side of vanadium enolate. However, as it appears from the optimized

DOI: 10.1021/jacs.7b01931
J. Am. Chem. Soc. 2017, 139, 10250−10266

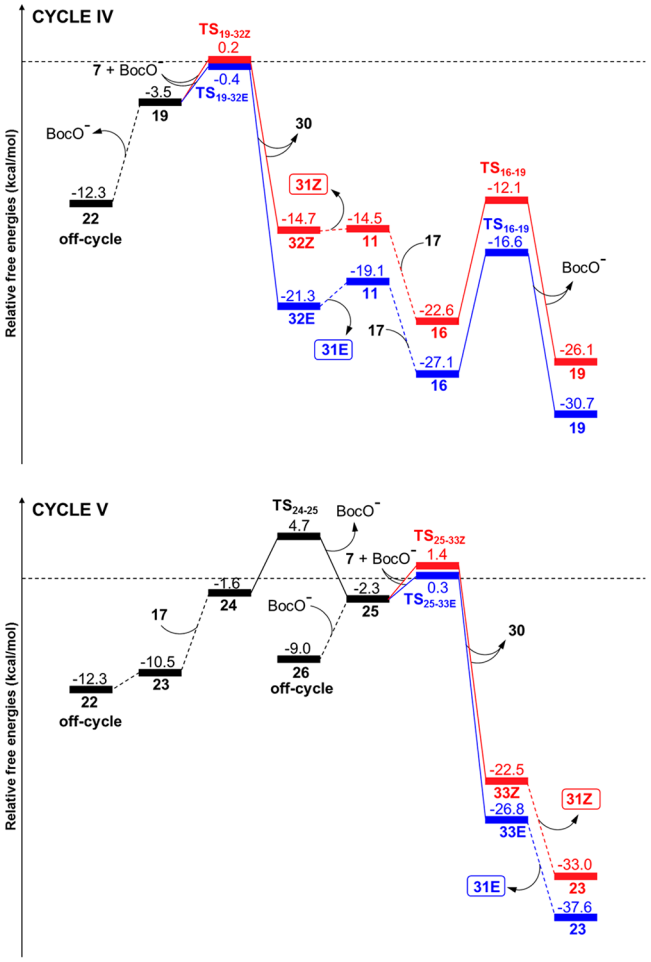

Figure 5. Free energy profiles for the palladium part of the combined reaction involving Pd(0)−Pd(0)/Pd(0)−Pd(II) (Cycle IV) and Pd(0)−Pd(II)/Pd(II)−Pd(II) (Cycle V) intermediates.

structures of $\mathbf{TS_{19-31E}}$ and $\mathbf{TS_{25-32E}}$ (Figure 6), the distortion caused by the presence of the phenyl group is not large, and it is, thus, compensated by other favorable interactions, such as for instance van der Waals attractions between the phenyl substituents on the ligands of vanadium and palladium.

The bicatalytic C−C bond formation via $\mathbf{TS_{19-32E}}$/$\mathbf{TS_{19-32Z}}$ and $\mathbf{TS_{25-33E}}$/$\mathbf{TS_{25-33Z}}$ yields palladium complexes containing coordinated products (**32E**/**32Z** and **33E**/**33Z**, respectively), accompanied by (t-BuOCO$_2$)(Ph$_3$SiO)$_2$VO (**30**). The catalytic cycles are closed by appropriate ligand exchange steps, which release the respective products and regenerate active palladium species **19** and **24**. Similarly, the active form of vanadium catalyst **5** is regenerated by an exchange of the carbonate ligand in intermediate **30** with a propargylic alcohol moiety, as described in the previous section (Scheme 8). Finally, the released carbonic acid monoester (BocOH) undergoes a subsequent decarboxylation outside the catalytic cycle via $\mathbf{TS_{BocOH-CO_2}}$, also as described above. Overall, the transformation of **1** and **17** into **31E** or **31Z** (and t-BuOH + CO$_2$) is exergonic by as much as 58.8 and 54.3 kcal/mol, respectively.

3.5. Overall Combined Mechanism and Analysis of Selectivity. The detailed DFT calculations described above disclose that the investigated reaction follows a very complex mechanism. In addition to the involvement of two catalysts and the necessity to account for the formation of three different products (two of them as mixtures of (E) and (Z) isomers), a major complication arises from the presence of dinuclear palladium complexes that according to the calculations may promote the C−O and C−C bond formations via two different pathways. The overall mechanism consists thus of seven interconnected and partially overlapping catalytic cycles (nine cycles if the (E)/(Z) options are counted separately), augmented with a number of additional off-cycle processes. An overview of the complete mechanism is given in Scheme 11 that contains the key intermediates and their transformations.

In the case of simple catalytic cycles, it is usually possible and relatively straightforward to determine rates and selectivities (product distributions) by a direct analysis of the corresponding free energy profiles. However, in the present case, the selectivity is determined by the relative rates of multiple pathways, some of them operating independently, while some being dependent on each other via the concentrations of common intermediates. Hence, the direct extraction of selectivity information from the diagrams shown in Figures 1, 4, and 5 is not possible. Moreover, it is also not feasible to apply the steady-state approximation to obtain the concentrations of the catalytic intermediates at a given progress of the reaction, since the presence of direct couplings between two catalytic intermediates (e.g., **7** + **19** and **7** + **25**) renders the equations defining the steady-state nonlinear. Therefore, we decided to resort to numerical kinetics simulations to retrieve information about the reaction selectivity from the computed energetics. By doing this, it is possible to directly link the results of the calculations with the experimental data. This kind of simulation technique has been extensively used to investigate the kinetic behavior of complex systems that involve large numbers of elementary reactions, for instance in combustion chemistry,[28] as well to study catalysis in heterogeneous systems.[29] On the contrary, examples of the application of kinetics simulations to the analysis of free energy surfaces obtained by quantum chemical calculations for homogeneously catalyzed reactions have only started to emerge recently.[30]

For the purpose of the simulations we used a kinetic network consisting of all reactions shown in Schemes 4, 8, and 10. All steps were treated as reversible, with the rate constants for forward and backward reactions calculated by the Eyring equation, using the barrier heights from the free energy diagrams (Figures 1, 4, and 5). For the reactions proceeding without a barrier, the rate constants were assumed to be equal to the pre-exponential coefficient of the Eyring equation, k_BT/h = 6.942 × 10^{12} M^{-1} s^{-1} (at 60 °C), in order to maintain the calculated thermodynamic energy differences.[31]

First, we carried out a series of kinetics simulations to assess how well the theoretically modeled reaction outcomes compare to the available experimental data. Although the reaction has not been subject to experimental kinetic investigations, the performed optimization experiments provide some quantitative information about how the ratio of products varies with changing catalyst loadings, and this can be used to compare with the theoretical model (Table 1).[2]

When examining the results of Table 1, one has to bear in mind the exponential dependence of the rates on relative free energies. That is, an error of 1.5 kcal/mol in the calculation of a given reaction barrier will translate into a 10-fold deviation in the simulated rate constant, which could have profound consequences on the overall product distribution. Error bars of this magnitude and larger are of course expected in the current calculations, due to the inherent inaccuracy of the

DOI: 10.1021/jacs.7b01931
J. Am. Chem. Soc. 2017, 139, 10250−10266

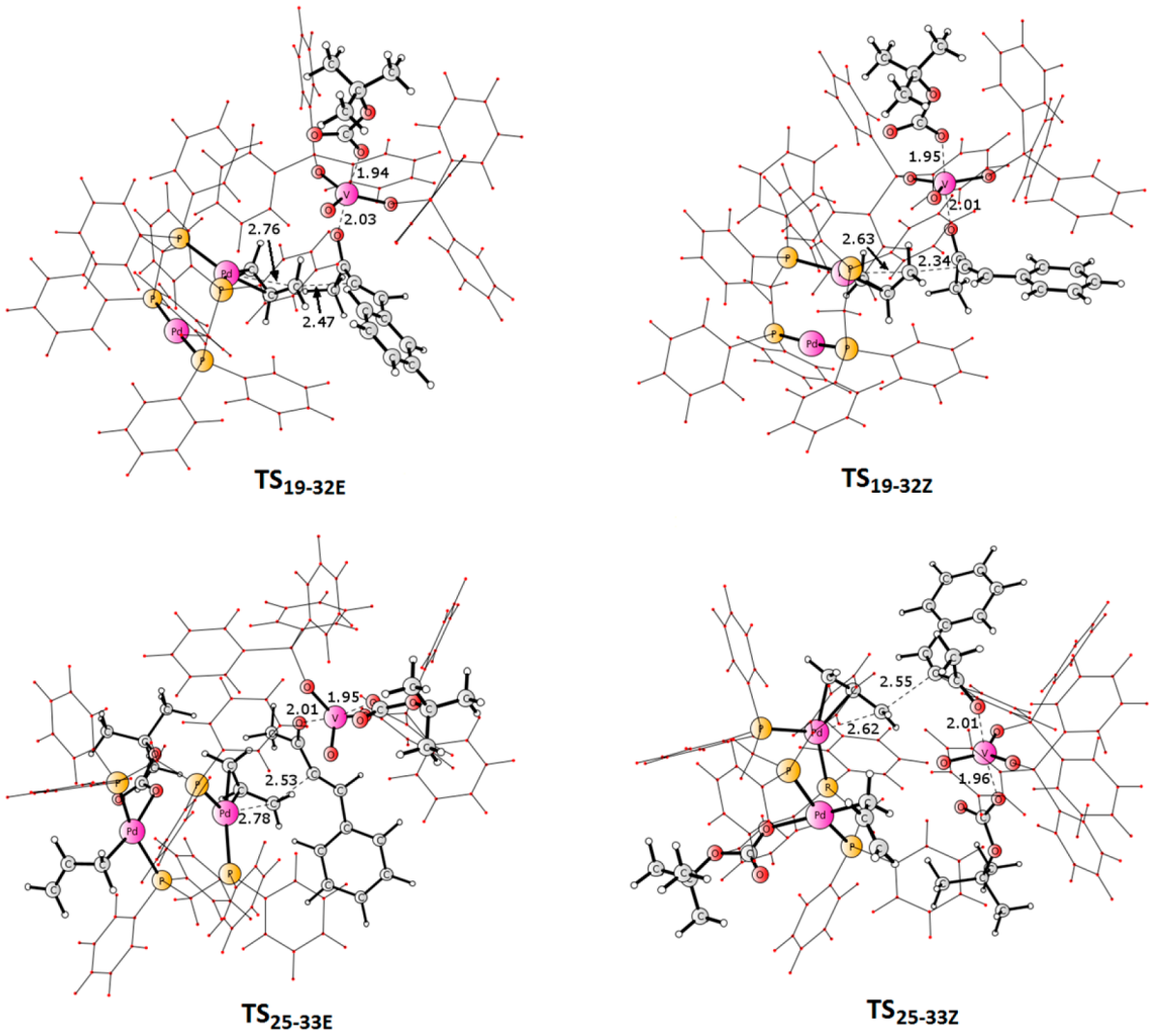

Figure 6. Optimized structures of transitions states for the key coupling between the vanadium enolate and the palladium π-allyl complexes. The backbones and phenyl groups of dppm ligands as well as Ph_3Si groups of vanadium catalyst are shown in a simplified fashion for clarity. Distances are given in Å.

underlying electronic structure methods and the modelistic approximations introduced (e.g., the truncation of substrate structure, possible errors in the conformational search, the ideal gas thermodynamic assumption, etc.). Considering all this, the agreement between the simulated and experimental values must be considered as outstanding. Namely, the general trends in the selectivity upon varying the catalyst amounts and ratios are correctly reproduced, and also the (*E*)/(*Z*)-isomers ratio for product **31** is predicted quite well (2.6:1−2.7:1 in the simulations vs 3:1−6:1 in the experiments). To some degree, the results could of course benefit from fortunate cancellation of errors. The amount of product **3** in entries 1 and 3 is, however, somewhat overestimated compared to the experimental outcome, which lead to some underestimation of the amounts of the other two products (especially **27** in entry 3).

Nevertheless, the results clearly demonstrate that the mechanism established by the calculations (Scheme 11) and the corresponding energy profiles are reliable and can be used for further analysis to gain deeper insights into the reaction and serve as a means the identify general factors controlling the overall selectivity.

To analyze how the amounts and ratios of the vanadium and palladium catalysts and the barriers for the various individual steps of the mechanism affect the selectivity, we carried out a sensitivity analysis, whose results are presented in Figure 7 and Table 2.

With increasing loading of the palladium catalyst (while keeping the vanadium amount constant), the simulations show that the ratio of products **3** and **31** gradually switches in favor of the latter one, whereas the amount of **27** consistently, but very slowly, grows (Figure 7a). In this respect, the simulations reproduce very the well experimental observations (Table 1, entries 1 and 2).

As far as the vanadium loading is concerned, its increase (while keeping the palladium amount constant) results in a lowering of the yield of **27** and a rise of the yields of **3** and **31** (Figure 7b). Interestingly, the changes in the selectivity are very pronounced in the low range of vanadium loadings (up to ∼0.5%), as the curves quickly converge, and further increase in the amount of the vanadium has little impact on the products ratio.

Most likely, the point at which the plots in Figure 7b flatten is slightly shifted toward lower vanadium loadings compared to

DOI: 10.1021/jacs.7b01931
J. Am. Chem. Soc. 2017, 139, 10250−10266

Scheme 11. Overview of the Overall Reaction Mechanism As Established by the Current Calculations[a]

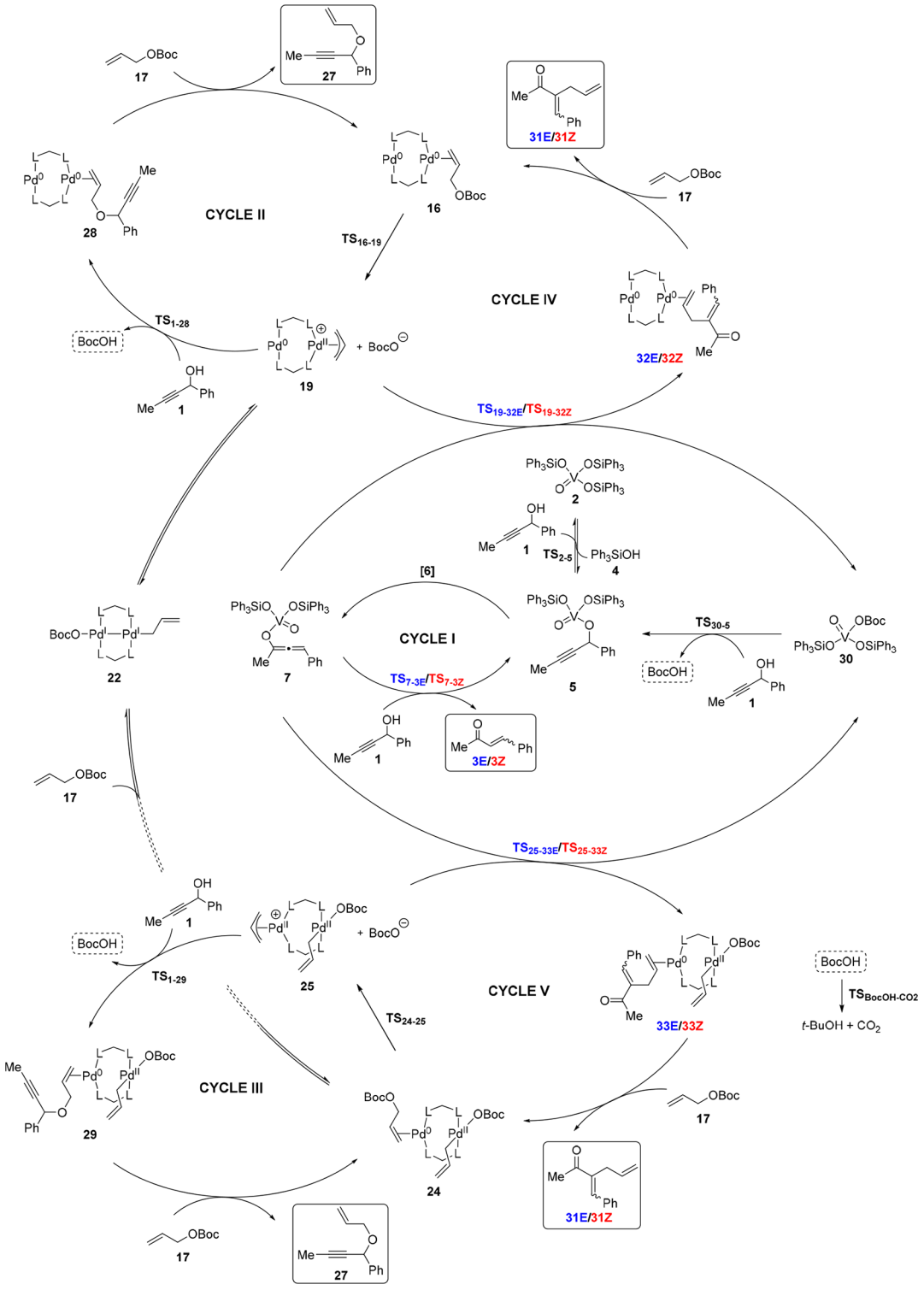

[a]Note that only selected key intermediates are shown here; see Schemes 4, 8, and 10 for detailed catalytic cycles. The pathways for the formation of ether **27**, involving intermediate **5** as the nucleophile, are entirely omitted, since they were found to contribute only negligible amounts of this product in the simulations (see the text for discussion).

its actual position due to inaccuracies in the calculated free energies. This in turn results in the above-mentioned underestimation of the amount of product **27** in the simulation vs the experimentally observed value (Table 1, entry 3). The fact that the selectivity of the cooperatively catalyzed reaction is affected differently upon varying the amounts of vanadium and palladium suggests different behaviors of the two catalysts in the combined network of reactions. This will be discussed further below.

Table 2 summarizes the results of a sensitivity analysis, in which the energy of selected TSs is raised or lowered by 1.52 kcal/mol, while the energies of all the other species were kept

DOI: 10.1021/jacs.7b01931
J. Am. Chem. Soc. 2017, 139, 10250−10266

Table 1. Simulated Selectivities with Varying Amounts of the Catalysts,[a] Corresponding to Conditions Tested Experimentally

			experimental product distribution[b]				simulated product distribution			
entry	V catalyst (mol %)	Pd catalyst (mol %)	3	27	31	31E:31Z	3	27	31	31E:31Z
1	5	5	6	2	92	3:1	27	4	69	2.6:1
2	5	1	64	2	34	6:1	61	1	38	2.7:1
3	1	5	3	40	57	3:1	25	9	66	2.6:1

[a]Initial concentrations: $[\mathbf{1}]_0 = [\mathbf{17}]_0 = 1.0$ M; simulations were run to 99% conversion of substrate **1**; amounts of products are normalized to 100. [b]Ref 2.

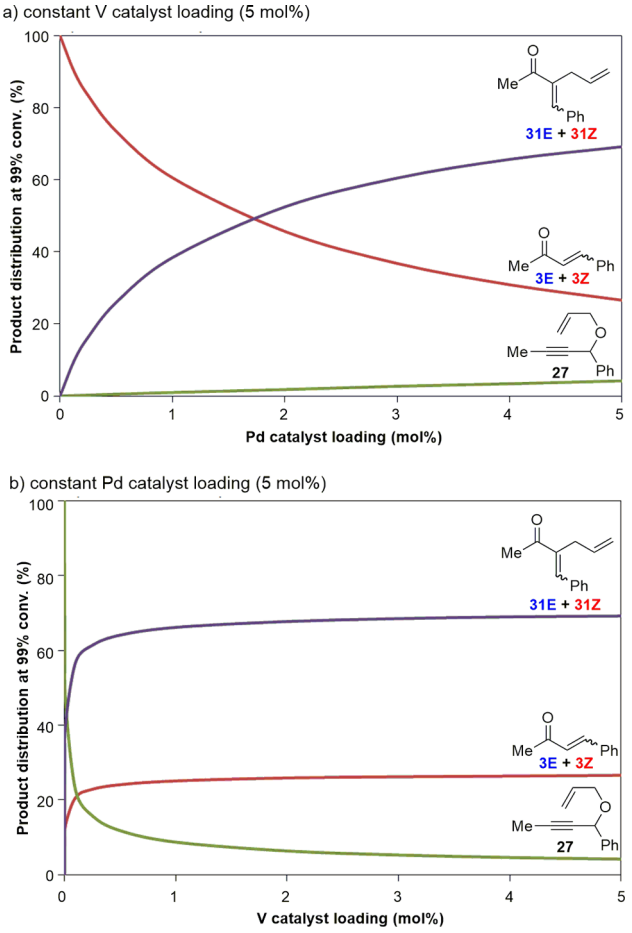

Figure 7. Dependence of the selectivity of the simulated reactions on the amount of (a) palladium and (b) vanadium catalysts. Initial concentrations are $[\mathbf{1}]_0 = [\mathbf{17}]_0 = 1$ M.

the same. Such a change in energy corresponds to a 10-fold decrease or increase in the rate constant for the respective elementary reaction at 60 °C.

From this analysis it is clear that the key transition states controlling the selectivity and affecting the amount of one product relative to the others are (1) transition ion-pair [**6**] (Table 2, entry 2; **3** and **31** combined vs **27**); (2) $\mathbf{TS}_{7-3E}$/$\mathbf{TS}_{7-3Z}$ (entry 3; **3** vs **31**, **27** not affected); (3) $\mathbf{TS}_{1-28}$ and $\mathbf{TS}_{1-29}$ (entries 5 and 8; **27** vs combined **3** and **31**); and (4) $\mathbf{TS}_{19-32E}$/$\mathbf{TS}_{19-32Z}$ and $\mathbf{TS}_{25-33E}$/$\mathbf{TS}_{25-33Z}$ (entries 10 and 11; **31** vs **3**, **27** not affected). The transition states for the formation of ether **27**, which involve vanadium alkoxide **5** as the nucleophile, $\mathbf{TS}_{5-28}$ and $\mathbf{TS}_{5-29}$, do not influence the final selectivity to any noticeable extent (entries 6 and 9). Interestingly, none of the transition states for the oxidative additions of allylic carbonate to Pd(0) ($\mathbf{TS}_{16-19}$ and $\mathbf{TS}_{24-25}$), the regeneration of vanadium catalyst ($\mathbf{TS}_{30-5}$), or the off-cycle decarboxylation ($\mathbf{TS}_{\mathbf{BocOH-CO_2}}$) have any noticeable impact on the selectivity either.

Another interesting issue is the alteration of the (*E*):(*Z*) ratio of product **31** resulting from the change in the energies of $\mathbf{TS}_{19-32E}$/$\mathbf{TS}_{19-32Z}$ and $\mathbf{TS}_{25-33E}$/$\mathbf{TS}_{25-33Z}$ (entries 10 and 11). It is caused by the different inherent (*E*):(*Z*) selectivities of Cycles IV and V, 2.4:1 and 5.0:1, respectively (*vide supra*), and their relative contributions to the overall formation of **31**. Namely, in the unmodified model (entry 1), Cycle IV contributes 85% of product **31**, while the more (*E*)-selective Cycle V only 15%, resulting in the combined 2.6:1 (*E*):(*Z*) selectivity. Upon variation in the relative energies of $\mathbf{TS}_{19-32E}$/$\mathbf{TS}_{19-32Z}$ and $\mathbf{TS}_{25-33E}$/$\mathbf{TS}_{25-33Z}$, these contributions change, leading to the accordingly modified final (*E*):(*Z*) ratio. Regarding product **27**, 45% originates from $\mathbf{TS}_{1-28}$ in Cycle II and 55% from $\mathbf{TS}_{1-29}$ in Cycle III. As a result of the very low concentration of vanadium alkoxide **5**, $\mathbf{TS}_{5-28}$ in Cycle II and $\mathbf{TS}_{5-29}$ in Cycle III (Scheme 8) contribute only a negligible amount of this side-product.

To rationalize the results of the simulations presented in Figure 7 and Table 2 and to further understand the overall kinetic behavior of the mechanistic model shown in Scheme 11, it is also instructive to examine the distributions of the different forms of vanadium and palladium catalysts in the reaction mixture. The simulations show that, irrespective of the initial conditions (e.g., catalysts loadings), the dominant vanadium-containing species throughout the reaction is complex **2**, accounting for the vast majority of vanadium (>99%). Complex **2** is the lowest laying intermediate, and the difference between its energy and the energy of ion-pair [**6**] constitutes the highest barrier for all the reactions involving vanadium (overall 26.8 kcal/mol, see Figures 1 and 5).

For the palladium catalyst, the dominant form and the resting state is the Pd(I)−Pd(I) complex **22**, also comprising >99% of palladium throughout the reaction. Complex **22** was indeed determined to be the most stable palladium complex in the calculations, and it also faces the highest overall barriers both in the O-allylation cycles (23.6 kcal/mol to $\mathbf{TS}_{1-28}$ and 23.1 kcal/mol to $\mathbf{TS}_{1-29}$, Figure 4) and in the bicatalytic cycles (11.9/12.5 kcal/mol to $\mathbf{TS}_{19-32E}$/$\mathbf{TS}_{19-32Z}$ and 17.0 kcal/mol to $\mathbf{TS}_{24-25}$, Figure 5).

Taken together, the above results suggest the following picture for the overall kinetics and selectivity of the reaction. The bottleneck for the formation of both products **3** and **31** is the supply of vanadium enolate **7** via the transition ion-pair [**6**]. Hence, the final amounts of these two products are influenced in a similar fashion by the changing of the vanadium loading (Figure 7b), which affects the rate at which **7** is formed,[32] and by the variation in the energy of [**6**] (Table 2, entry 2). Once formed, **7** reacts fast either with intermediates **19** or **25** via $\mathbf{TS}_{19-32E}$/$\mathbf{TS}_{19-32Z}$ and $\mathbf{TS}_{25-33E}$/$\mathbf{TS}_{25-33Z}$ to eventually give product **31** or with alcohol **1** via $\mathbf{TS}_{7-3E}$/$\mathbf{TS}_{7-3Z}$ to produce **3**.

DOI: 10.1021/jacs.7b01931
J. Am. Chem. Soc. 2017, 139, 10250−10266

Table 2. Effect of Increasing or Decreasing the Energy of Selected Transition States on the Product Distribution[a]

		raised by 1.52 kcal/mol				lowered by 1.52 kcal/mol			
entry	modified TS	3	27	31	31E:31Z	3	27	30	31E:31Z
1	none	27	4	69	2.6:1	27	4	69	2.6:1
2	[6]	19	28	53	2.6:1	28	0	72	2.6:1
3	TS_{7-3E}/TS_{7-3Z}[b]	4	4	92	2.6:1	70	5	25	2.7:1
4	TS_{16-19}	27	4	69	2.6:1	27	4	69	2.6:1
5	TS_{1-28}	27	3	70	2.6:1	23	16	61	2.6:1
6	TS_{5-28}	27	4	69	2.6:1	27	4	69	2.6:1
7	TS_{24-25}	27	4	69	2.6:1	27	4	69	2.6:1
8	TS_{1-29}	27	2	71	2.6:1	21	20	59	2.6:1
9	TS_{5-29}	27	4	69	2.6:1	27	4	69	2.6:1
10	TS_{19-32E}/TS_{19-32Z}[b]	53	5	42	3.8:1	5	4	91	2.4:1
11	TS_{25-33E}/TS_{25-33Z}[b]	30	4	66	2.4:1	14	4	82	3.5:1
12	TS_{30-5}	27	4	69	2.6:1	27	4	69	2.6:1
13	$TS_{BocOH-CO_2}$	27	4	69	2.6:1	27	4	69	2.6:1

[a]Initial concentrations: $[1]_0 = [17]_0 = 1.0$ M, $[2]_0 = 0.05$ M, $[11]_0 = 0.025$ M; simulations were run to 99% conversion of substrate **1**; amounts of products are normalized to 100. [b]Energies of both transition states were modified simultaneously.

It is thus clear that the relative energies of these six transition states are decisive for the **3**:**31** ratio (Table 2, entries 3, 10, and 11). Since the palladium catalyst loading translates directly into the amounts of **19** and **25** present in the reaction mixture, an increase in the palladium loading results in a favorable formation of **31** relative to **3** and *vice versa* (Figure 7a). The situation regarding the formation of product **27** is somewhat different. Due to the approximately constant amounts of **19** and **25**[33] present in the mixture over the entire duration of the reaction, Cycles II and III operate at practically constant turnover rates independent of the other processes occurring elsewhere in the mechanisms. Thus, the final amount of **27** is mainly controlled by the amount of other products that Cycles I, IV, and V generate before substrate **1** is depleted. Since the limiting factor for all these three cycles is the vanadium-catalyzed supply of enolate **7**,[32] a large increase in the yield of **27** is observed with the decreasing of the vanadium catalyst loading (Figure 7b). The rate at which of **27** forms rises (practically linearly) with the palladium loading, but, at least in the simulations with 5% vanadium present in the reaction mixture, its final amount remains small (Figure 7a). Naturally, the selectivity between **27** and (**3** + **31**) is also affected by the relative energies of transition states [**6**], TS_{1-28}, and TS_{1-29} (Table 2, entries 2, 5, and 8).

In summary, the above analysis shows that the overall selectivity of the reaction cooperatively catalyzed by vanadium and palladium (Scheme 1) has a complex origin. Not surprisingly, it is controlled by the relative rates of the pathways diverging from the common intermediates **7**, **19**, and **25**. The selectivity is also strongly dependent on the rate at which intermediate **7** is supplied. On the other hand, the rates of formation of **19** and **25** are completely irrelevant in this respect, as their low concentrations, necessary to prevent the excessive generation of side-product **27**, are rather the result of the position of equilibrium between these two species and the palladium resting state **22**. Therefore, the results show that the earlier considerations regarding the conditions that need to be fulfilled for the successful synergistic catalysis are only partially correct.[2] Namely, to attain the desired transformation in high yield, it is indeed necessary that the coupling between the two catalytic intermediates outcompetes possible side processes, but the rates of supply of these intermediates may or may not be relevant for the selectivity of the reaction.

4. CONCLUSIONS

The coupling of propargylic alcohols with allylic carbonates cooperatively catalyzed by vanadium and palladium was subject to a thorough investigation using DFT calculations. We have established plausible catalytic cycles for the three processes comprising the overall mechanism, i.e., the vanadium-catalyzed Meyer−Schuster rearrangement, the palladium-catalyzed Tsuji−Trost O-allylation, and the bicatalytic coupling pathway. Of particular interest are the findings regarding the involvement of dinuclear palladium complexes in the mechanism of the reaction that sheds light on the general modes of activation of allylic, and potentially other, substrates by these type of species. The calculations disclose that the pathway engaging simultaneously both palladium centers is energetically disfavored compared to the mechanism wherein one palladium atom participates in the transformations, while the other is a spectator. Interestingly, the spectator center may adopt either 0 or II oxidation state, resulting in two distinct catalytic cycles, which may contribute to the formation of the products.

Due to the complexity of the combined mechanism, retrieving the reaction selectivity by analysis of the calculated free energy profiles or by application of the steady-state approximation is not possible. Therefore, we carried out kinetics simulations that create a direct link between the DFT calculations and experimental results. The simulations provided important insights into many aspects of the mechanism and its dynamics and enabled a detailed analysis of the sources of reaction selectivity. Moreover, the results of the simulations offer practical guidance for optimizing the reaction conditions in terms of the catalyst loadings and uncover the importance of the individual steps of the catalytic cycles on the selectivity and efficiency, thus pointing to possible improvements in the catalytic system. Although the investigated reaction represents a specific case, the results provide a general framework for understanding the kinetic behavior of reactions involving the cooperative catalysis. Thus, we believe that this contribution will have a bearing on the design of new catalytic systems based on this concept.

Finally, this work demonstrates the practical usefulness of DFT calculations for the investigation of both molecularly large (>200 atoms) and mechanistically complex systems. The calculated energies are of a sufficient accuracy to correctly

DOI: 10.1021/jacs.7b01931
J. Am. Chem. Soc. 2017, 139, 10250−10266

reproduce experimental selectivities, even in the case where these result from a convolution of many individual, chemically diverse, steps. We expect that the use of a combination of DFT calculations and kinetics simulations will increase in the future, as a growing number of reactions with increasing levels of complexity are being studied computationally and the analysis of the obtained data may not always be straightforward, especially in cases where the effect of concentrations needs to be taken into account.

■ ASSOCIATED CONTENT

Supporting Information

The Supporting Information is available free of charge on the ACS Publications website at DOI: 10.1021/jacs.7b01931.

Complete citation for ref 8; results of additional calculations not included in the article; details of the kinetic model used in the simulations; investigation of the mechanism and selectivity of the reaction employing dppe ligand; calculated energies and energy corrections for all the species; optimized structures and Cartesian coordinates of stationary points (PDF)

■ AUTHOR INFORMATION

Corresponding Authors

*m.kalek@cent.uw.edu.pl
*fahmi.himo@su.se

ORCID

Marcin Kalek: 0000-0002-1595-9818
Fahmi Himo: 0000-0002-1012-5611

Notes

The authors declare no competing financial interest.

■ ACKNOWLEDGMENTS

We thank Prof. Barry Trost for valuable discussions on the mechanism. We acknowledge financial support from the Swedish Research Council, the Göran Gustafsson Foundation, the Knut and Alice Wallenberg Foundation, and the National Science Centre, Poland (grant no.: 2014/15/D/ST5/02579). Computer time was generously provided by the Swedish National Infrastructure for Computing.

■ REFERENCES

(1) (a) Wang, M. H.; Scheidt, K. A. *Angew. Chem., Int. Ed.* **2016**, *55*, 14912−14922. (b) *Cooperative Catalysis: Designing Efficient Catalysts for Synthesis*; Peters, E. L., Ed.; Wiley-VCH: Weinheim, 2015. (c) Allen, A. E.; MacMillan, D. W. C. *Chem. Sci.* **2012**, *3*, 633−658. (d) Cohen, D. T.; Scheidt, K. A. *Chem. Sci.* **2012**, *3*, 53−57. (e) Zhong, C.; Shi, X. *Eur. J. Org. Chem.* **2010**, *2010*, 2999−3025. (f) Rueping, M.; Koenigs, R. M.; Atodiresei, I. *Chem. - Eur. J.* **2010**, *16*, 9350−9365. (g) Shao, Z.; Zhang, H. *Chem. Soc. Rev.* **2009**, *38*, 2745−2755. (h) Ma, J.-A.; Cahard, D. *Angew. Chem., Int. Ed.* **2004**, *43*, 4566−4583.

(2) (a) Trost, B. M.; Luan, X. *J. Am. Chem. Soc.* **2011**, *133*, 1706−1709. (b) Trost, B. M.; Luan, X.; Miller, Y. *J. Am. Chem. Soc.* **2011**, *133*, 12824−12833.

(3) For selected examples of other reactions catalyzed cooperatively by two metals see: (a) Sonogashira, K.; Tohda, Y.; Hagihara, N. *Tetrahedron Lett.* **1975**, *16*, 4467−4470. (b) Sawamura, M.; Sudoh, M.; Ito, Y. *J. Am. Chem. Soc.* **1996**, *118*, 3309−3310. (c) Li, C.-J.; Wei, C. *Chem. Commun.* **2002**, 268−269. (d) Sammis, G. M.; Danjo, H.; Jacobsen, E. N. *J. Am. Chem. Soc.* **2004**, *126*, 9928−9929. (e) Hirner, J. J.; Shi, Y.; Blum, S. A. *Acc. Chem. Res.* **2011**, *44*, 603−613. (f) Yang, S.; Rui, K.-H.; Tang, X.-Y.; Xu, Q.; Shi, M. *J. Am. Chem. Soc.* **2017**, *139*, 5957−5964.

(4) Pauling, H.; Andrews, D. A.; Hindley, N. C. *Helv. Chim. Acta* **1976**, *59*, 1233−1243.

(5) See for example: (a) Sperger, T.; Sanhueza, I. A.; Schoenebeck, F. *Acc. Chem. Res.* **2016**, *49*, 1311−1319. (b) Zhang, X.; Chung, L. W.; Wu, Y.-D. *Acc. Chem. Res.* **2016**, *49*, 1302−1310. (c) Balcells, D.; Clot, E.; Eisenstein, O.; Nova, A.; Perrin, L. *Acc. Chem. Res.* **2016**, *49*, 1070−1078. (d) Santoro, S.; Kalek, M.; Huang, G.; Himo, F. *Acc. Chem. Res.* **2016**, *49*, 1006−1018. (e) Lam, Y.; Grayson, M. N.; Holland, M. C.; Simon, A.; Houk, K. N. *Acc. Chem. Res.* **2016**, *49*, 750−762. (f) Sperger, T.; Sanhueza, I. A.; Kalvet, I.; Schoenebeck, F. *Chem. Rev.* **2015**, *115*, 9532−9586. (g) Tsang, A. S.-K.; Sanhueza, I. A.; Schoenebeck, F. *Chem. - Eur. J.* **2014**, *20*, 16432−16441. (h) Sameera, W. M. C.; Maseras, F. *WIREs Comput. Mol. Sci.* **2012**, *2*, 375−385. (i) Cheong, P. H-A.; Legault, C. Y.; Um, J. M.; Çelebi-Ölçüm, N.; Houk, K. N. *Chem. Rev.* **2011**, *111*, 5042−5137.

(6) For examples of application of the steady-state approximation to simpler reaction networks see: (a) Christiansen, J. A. *Adv. Catal.* **1953**, *5*, 311−353. (b) Blackmond, D. G.; Hodnett, N. S.; Lloyd-Jones, G. C. *J. Am. Chem. Soc.* **2006**, *128*, 7450−7451. (c) Kozuch, S.; Shaik, S. *Acc. Chem. Res.* **2011**, *44*, 101−110. (d) Kozuch, S. *WIREs Comput. Mol. Sci.* **2012**, *2*, 795−815. (e) Rush, L. E.; Pringle, P. G.; Harvey, J. N. *Angew. Chem., Int. Ed.* **2014**, *53*, 8672−8676.

(7) (a) Lee, C.; Yang, W.; Parr, R. G. *Phys. Rev. B: Condens. Matter Mater. Phys.* **1988**, *37*, 785−789. (b) Becke, A. D. *Phys. Rev. A: At., Mol., Opt. Phys.* **1988**, *38*, 3098−3100. (c) Becke, A. D. *J. Chem. Phys.* **1992**, *96*, 2155−2160. (d) Becke, A. D. *J. Chem. Phys.* **1992**, *97*, 9173−9177. (e) Becke, A. D. *J. Chem. Phys.* **1993**, *98*, 5648−5652.

(8) Frisch, M. J.; et al. *Gaussian 09*, Revision A.02; Gaussian, Inc.: Wallingford, CT, 2009.

(9) Hay, P. J.; Wadt, W. R. *J. Chem. Phys.* **1985**, *82*, 270−283.

(10) (a) Grimme, S.; Antony, J.; Ehrlich, S.; Krieg, H. *J. Chem. Phys.* **2010**, *132*, 154104−22. (b) Grimme, S.; Ehrlich, S.; Goerigk, L. *J. Comput. Chem.* **2011**, *32*, 1456−1465.

(11) (a) Barone, V.; Cossi, M. *J. Phys. Chem. A* **1998**, *102*, 1995−2001. (b) Cossi, M.; Rega, N.; Scalmani, G.; Barone, V. *J. Comput. Chem.* **2003**, *24*, 669−681.

(12) Plata, R. E.; Singleton, D. A. *J. Am. Chem. Soc.* **2015**, *137*, 3811−3826.

(13) Petzold, L. *SIAM J. Sci. Stat. Comput.* **1983**, *4*, 136−148.

(14) Hindmarsh, A. C. ODEPACK, A Systematized Collection of ODE Solvers. In *IMACS Transactions on Scientific Computation Vol. 1: Scientific Computing*; Stepleman, R. S., Ed.; North-Holland: Amsterdam, 1983; pp 55−64.

(15) Hoops, S.; Sahle, S.; Gauges, R.; Lee, C.; Pahle, J.; Simus, N.; Singhal, M.; Xu, L.; Mendes, P.; Kummer, U. *Bioinformatics* **2006**, *22*, 3067−3074.

(16) Kalek, M.; Himo, F. *J. Am. Chem. Soc.* **2012**, *134*, 19159−19169.

(17) (a) Ernan, M. B.; Aul'chenko, I. S.; Kheifits, L. A.; Dulova, V. G.; Novikov, J. N.; Vol'pin, M. E. *Tetrahedron Lett.* **1976**, *17*, 2981−2984. (b) Olson, G. L.; Morgan, K. D.; Saucy, G. *Synthesis* **1976**, *1976*, 25−26. (c) Trost, B. M.; Oi, S. *J. Am. Chem. Soc.* **2001**, *123*, 1230−1231. (d) Trost, B. M.; Chung, C. K. *J. Am. Chem. Soc.* **2006**, *128*, 10358−10359.

(18) (a) Mackenzie, P. B.; Whelan, J.; Bosnich, B. *J. Am. Chem. Soc.* **1985**, *107*, 2046−2054. (b) Vitagliano, A.; Åkermark, B. *J. Organomet. Chem.* **1988**, *349*, C22−C26. (c) Ramdeehul, S.; Dierkes, P.; Aguado, R.; Kamer, P. C. J.; van Leeuwen, P. W. N. M.; Osborn, J. A. *Angew. Chem., Int. Ed.* **1998**, *37*, 3118−3121. (d) Amatore, C.; Jutand, A.; Meyer, G.; Mottier, L. *Chem. - Eur. J.* **1999**, *5*, 466−473. (e) Kuhn, O.; Mayr, H. *Angew. Chem., Int. Ed.* **1999**, *38*, 343−346. (f) Amatore, C.; Gamez, S.; Jutand, A. *Chem. - Eur. J.* **2001**, *7*, 1273−1280. (g) Amatore, C.; Bahsoun, A. A.; Jutand, A.; Mensah, L.; Meyer, G.; Ricard, L. *Organometallics* **2005**, *24*, 1569−1577. (h) Amatore, C.; Génin, E.; Jutand, A.; Mensah, L. *Organometallics* **2007**, *26*, 1875−1880. (i) Evans, L. A.; Fey, N.; Harvey, J. N.; Hose, D.; Lloyd-Jones, G. C.; Murray, P.; Orpen, A. G.; Osborne, R.; Owen-Smith, G. J. J.; Purdie, M. *J. Am. Chem. Soc.* **2008**, *130*, 14471−14473.

DOI: 10.1021/jacs.7b01931
J. Am. Chem. Soc. 2017, 139, 10250−10266

(19) (a) Kleimark, J.; Norrby, P.-O. Computational Insights into Palladium-Mediated Allylic Substitution Reactions. In *Topics in Organometallic Chemistry*; Kazmaier, U., Ed.; Springer-Verlag: Berlin, 2012; Vol. *38*, pp 65−93. (b) Cardenas, D. J.; Echavarren, A. M. *New J. Chem.* **2004**, *28*, 338−347. (c) Keith, J. A.; Behenna, D. C.; Sherden, N.; Mohr, J. T.; Ma, S.; Marinescu, S. C.; Nielsen, R. J.; Oxgaard, J.; Stoltz, B. M.; Goddard, W. A., III *J. Am. Chem. Soc.* **2012**, *134*, 19050−19060.

(20) For a review with leading references, see: *Handbook of Organopalladium Chemistry for Organic Synthesis*; Negishi, E., Ed.; Wiley−Interscience: New York, 2002; Vol. *2*, pp 1663−2027.

(21) Reviews: (a) Puddephatt, R. J. *Chem. Soc. Rev.* **1983**, *12*, 99−127. (b) Murahashi, T.; Kurosawa, H. *Coord. Chem. Rev.* **2002**, *231*, 207−228. Representative examples: (c) Holloway, R. G.; Penfold, B. R.; Colton, R.; McCormick, M. J. *J. Chem. Soc., Chem. Commun.* **1976**, 485−486. (d) Benner, L. S.; Balach, A. L. *J. Am. Chem. Soc.* **1978**, *100*, 6099−6106. (e) Lindsay, C. H.; Balch, A. L. *Inorg. Chem.* **1981**, *20*, 2267−2270. (f) Krafft, T. E.; Hejna, C. I.; Smith, J. S. *Inorg. Chem.* **1990**, *29*, 2682−2688. (g) Maekawa, M.; Munakata, M.; Kuroda-Sowa, T.; Suenaga, Y. *Inorg. Chim. Acta* **1998**, *281*, 116−119. (h) Besenyei, G.; Parkanyi, L.; Gacs-Baitz, E.; James, B. R. *Inorg. Chim. Acta* **2002**, *327*, 179−187.

(22) For representative examples, see: (a) Refs 21a and 21e. (b) Palenik, G. J.; Mathew, M.; Steffen, W. L.; Beran, G. *J. Am. Chem. Soc.* **1975**, *97*, 1059−1066. (c) Steffen, W. L.; Palenik, G. J. *Inorg. Chem.* **1976**, *15*, 2432−2439.

(23) The complexation of palladium by (*E*),(*E*)-dibenzylideneacetone (dba), originating from the precatalyst, is not considered in the current study. Although it has been shown to occur in stoichiometric investigations (see refs 18d, f, and g), under the catalytic conditions, the involvement of dba in the mechanism should be negligible due to much higher concentrations of other unsaturated species in the reaction mixture.

(24) The formation of π-allyl bridged Pd(I)−Pd(I) complexes could not be observed in the investigated $(dppm)_2Pd_2$ system. Complexes of this type were reported for dinuclear palladium complexes containing other auxiliary ligands, for examples and leading references see: (a) Werner, H. *Adv. Organomet. Chem.* **1981**, *19*, 155−182. (b) Murahashi, T.; Kurosawa, H. *Coord. Chem. Rev.* **2002**, *231*, 207−228. (c) Tromp, M.; Sietsma, J. R. A.; van Bokhoven, S. A.; van Strijdonck, G. P. F.; van Haaren, R. J.; van der Eerden, A. M. J.; van Leeuwen, P. W. N. M.; Koningsberger, D. C. *Chem. Commun.* **2003**, 128−129. (d) Markert, C.; Neuburger, M.; Kulicke, K.; Meuwly, M.; Pfaltz, A. *Angew. Chem., Int. Ed.* **2007**, *46*, 5892−5895.

(25) The calculated energy of complex **19** with a loosely bound *tert*-butyl carbonate anion included in the structure is higher by 3.6 kcal/mol compared to a fully dissociated cation **19** and $BocO^-$ anion.

(26) It was found that the decarboxylation of carbonic acid is efficiently catalyzed by a proton shuttle, transferring the proton between the oxygen atoms of BocOH. This role may be played by either of the alcohols present in the reaction mixture (substrate **1** or *t*-butanol, generated as a side product) or by another molecule of the carbonic acid. The calculations show that the latter alternative is more facile, resulting in a 14.0 kcal/mol barrier, compared to >20 kcal/mol in the case of alcohols playing the role of the proton shuttle (see Supporting Information for details).

(27) For comparative reasons we have calculated a full mechanism for the reaction depicted in Scheme 1, but with dppe ligand instead of dppm. In this case, the cycles for the palladium-catalyzed O-allylation of propargylic alcohol **1** and the cooperatively catalyzed combined reaction involve mononuclear palladium complexes, but they consist of otherwise similar steps as those in the mechanism established for dppm (Schemes 8 and 10). Analysis of the free energy profiles corresponding to these cycles reveals that the mononuclear π-allyl complexes display lower intrinsic reactivity toward nucleophiles (both alcohol **1** and vanadium enolate **7**) compared to the corresponding dinuclear complexes with dppm, with the barriers higher by as much as 5−10 kcal/mol. In terms of the overall energy spans (all the way from the resting state to the highest transition state), the differences are smaller, but amount to 2−4 kcal/mol. Since the catalytic cycle for the vanadium-catalyzed Meyer−Schuster rearrangement is identical in both cases (Scheme 4 and Figure 1), ketone **3** becomes the major product in the kinetics simulations of the reaction employing dppe. Thus, the computed selectivity is in line with the experimentally observed one (see, ref 2b). Detailed computational characterization of the mechanism with dppe ligand is provided in the Supporting Information.

(28) *J. Phys. Chem.* **1977**, *81* (25). This issue contains many articles on applications of numerical simulations in chemical kinetics. More recently, simulations were for instance used to examine different scenarios that may occur during kinetic resolutions, see for example: (a) Ref 6d. (b) Dominguez, B.; Hodnett, N. S.; Lloyd-Jones, G. C. *Angew. Chem., Int. Ed.* **2001**, *40*, 4289−4291. (c) Satyanarayana, T.; Kagan, H. B. *Tetrahedron* **2007**, *63*, 6415−6422. (d) Fransson, L.; Laurell, A.; Widyan, K.; Wingstrand, E.; Hult, K.; Moberg, C. *ChemCatChem* **2010**, *2*, 683−693.

(29) For examples, see: (a) Kandoi, S.; Greeley, J.; Sanchez-Castillo, M.; Evans, S.; Gokhale, A.; Dumesic, J.; Mavrikakis, M. *Top. Catal.* **2006**, *37*, 17−28. (b) Novell-Leruth, G.; Ricart, J. M.; Pérez-Ramírez, J. *J. Phys. Chem. C* **2008**, *112*, 13554−13562. (c) Teschner, D.; Novell-Leruth, G.; Farra, R.; Knop-Gericke, A.; Schlögl, R.; Szentmiklósi, L.; Hevia, M. G.; Soerijanto, H.; Schomäcker, R.; Pérez-Ramírez, J.; López, N. *Nat. Chem.* **2012**, *4*, 739−745.

(30) For examples, see: (a) Goehry, C.; Besora, M.; Maseras, F. *ACS Catal.* **2015**, *5*, 2445−2451. (b) Fernández-Alvarez, V. M.; Nappi, M.; Melchiorre, P.; Maseras, F. *Org. Lett.* **2015**, *17*, 2676−2679.

(31) A full description of the kinetic model used in the simulations, including a list of the reactions with the corresponding rate constants, is given in the Supporting Information.

(32) The rate of formation of **7** displays a square-root dependence on the vanadium loading. See the Supporting Information for details.

(33) The amount of **25** decreases steadily as the reaction progresses, due to the depletion of substrate **17**. In turn, the relative contribution of Cycle IV vs Cycle V to the formation of product **31** steadily increases. The same applies to Cycle II vs Cycle III, regarding the formation of product **27**.

DOI: 10.1021/jacs.7b01931
J. Am. Chem. Soc. 2017, 139, 10250−10266